ARTICLE IN PRESS

Chemical Engineering Journal xxx (xxxx) xxxx

Contents lists available at ScienceDirect

Chemical Engineering Journal

journal homepage: www.elsevier.com/locate/cej

Review

Recent progress in sustainable technologies for adsorptive and reactive removal of sulfonamides

Suhong Tian[a,b], Chen Zhang[a,b,*], Danlian Huang[a,b,*], Rongzhong Wang[a], Guangming Zeng[a,b], Ming Yan[a,b], Weiping Xiong[a,b], Chengyun Zhou[a,b], Min Cheng[a,b], Wenjing Xue[a,b], Yang Yang[a,b], Wenjun Wang[a,b]

[a] College of Environmental Science and Engineering, Hunan University, Changsha 410082, PR China
[b] Key Laboratory of Environmental Biology and Pollution Control, Ministry of Education, Hunan University, Changsha 410082, PR China

HIGHLIGHTS

- Conduct detailed analysis and discussion on the removal mechanisms.
- Solution pH and matrix components can significantly influence sulfonamides removal.
- Predominant degradation pathways are hydroxylation and the cleavage of S-N bond.
- Carbon-based materials may be good alternatives in the catalytic system.
- Research priorities and knowledge gaps are reviewed in removing sulfonamides.

ARTICLE INFO

Keywords:
Sulfonamide antibiotics
Pyrogenic carbonaceous materials
Advanced oxidation processes
Degradation pathway
Toxicity

ABSTRACT

The growing concerns over the environmental toxicity of sulfonamides (SNs) require immediate action to establish efficient and sustainable processes to address this issue. Adsorption, photodegradation and Fenton/Fenton-like reactions are the most applied processes to remove SNs. However, the adsorption behavior, degradation mechanisms and toxicity of intermediates need further investigation to guide engineering applications. The review focuses on the recent progress and challenges on adsorption, photodegradation and Fenton/Fenton-like techniques for SNs removal. In addition, influences of solution pH and matrix components on adsorption mechanisms are discussed. In particular, the degradation pathway of SNs and toxicity assessment of their intermediates are also analyzed. Finally, conclusions and research gaps in this field are briefly proposed. Publications on this topic have grown exponentially over the last decade. This review provides a unique and comprehensive environmental perspective, as well as the latest knowledge on SNs adsorption and reactive removal by different technologies.

1. Introduction

Antibiotics, discovered by Fleming in 1929, are the most commonly used drugs to treat bacterial infections in animals and humans [1–3]. Nowadays, it is widely used in livestock and aquaculture as growth promoters, which far more than their medical use. The usage of antibiotics worldwide has increased by 65% between 2000 and 2015 [4]. In 2013, China consumed 2.48×10^5 tons of antibiotics and discharged about 5.0×10^4 tons into water and soil [5]. Historically, sulfonamides (SNs) have been used for the longest time as synthetic antibiotics to treat protozoan and bacterial infections. SNs were the first antibiotics to be used systemically and paved the way for the revolution of antibiotics in biomedicine [6]. Nowadays, many SN derivatives have also been applied in agriculture. Because they are more efficient to against

Abbreviations: SNs, Sulfonamides; TMP, Trimethoprim; SMX, Sulfamethoxazole; SMZ, Sulfamethazine; STZ, Sulfathiazole; SDZ, Sulfadiazine; SFZ, Sulfamethizole; SCP, Sulfachloropyridazine; SSZ, Sulfasalazine; SPD, Sulfapyridine; SDM, Sulfadimethoxine; SSX, Sulfisoxazole; SMR, Sulfamerazine; AOP, Advanced oxidation process; PCM, Pyrogenic carbonaceous matter; GE, Graphene; GO, Graphene oxide; rGO, Reduced graphene oxide; BC, Biochar; AC, Activated carbon; PAC, Powdered activated carbon; CNT, Carbon nanotube; MWCNT, Multi-walled carbon nanotube; MOF, Metal-organic framework; g-C_3N_4, Graphitic carbon nitride; PDS, Peroxydisulfate

* Corresponding authors at: College of Environmental Science and Engineering, Hunan University, Changsha, Hunan 410082, PR China.
E-mail addresses: zhangchen@hnu.edu.cn (C. Zhang), huangdanlian@hnu.edu.cn (D. Huang).

https://doi.org/10.1016/j.cej.2019.123423
Received 11 May 2019; Received in revised form 20 September 2019; Accepted 6 November 2019
1385-8947/

bacterial infections, especially when organisms multiply rapidly [7]. *European Medicines Agency* pointed out that SNs were the third most used veterinary antibiotics in Europe in 2014, accounting for 11% of total veterinary antibiotic sales [8].

However, SNs are discharged into the environment as the parent compounds or metabolites due to its weakly absorbed or incomplete metabolism. Because of the high environmental mobility, SNs are often detected in natural environment [3,9,10]. The environment with low concentration levels of SNs could induce genetic mutations in bacteria, resulting in the formation of SN resistant bacteria [1,11]. In addition, SN residues in the environment pose potential risk to the environment and human health, inhibit the growth and survival of microorganisms, as well as accumulate in plants due to their high biological activity [12,13]. Therefore, it is of great significance to conduct a comprehensive study to develop novel, efficient and sustainable technologies for removing SNs and their derivatives.

Nowadays, numerous techniques, including biological process [14,15], adsorption [16] and advanced oxidation processes (AOPs) containing photocatalysis, Fenton/Fenton-like reaction, ultraviolet (UV) irradiation and electrochemical oxidation [17–20] have been used to remove antibiotics. Among them, adsorption and AOPs have been widely used over the past decade. Adsorption is a simple, environmental-friendly and scale-up method [21–23]. AOPs could convert contaminants into simple and nontoxic molecules through strong oxidizing free radicals (hydroxyl radical (•OH), sulfate radical ($SO_4^{\bullet -}$) and superoxide radical ($O_2^{\bullet -}$) etc.) [24,25], which possess a high removal efficiency. However, the adsorption mechanisms, degradation mechanisms and toxicity of intermediates need further investigation to guide engineering applications. Therefore, the paper discusses the environmental behavior of SNs and their removal mechanism by adsorption and AOPs, as well as providing useful guidelines on the removal of contaminants with similar physicochemical properties.

2. Occurrence and environmental behavior of sulfonamides

SNs are derivatives of p-aminobenzonic sulfonic acid, containing benzene ring, p-aminobenzic acid and sulfonic acid groups. Various chemical groups replace R groups to form derivatives with different physicochemical properties. According to the heterocyclic R group type, SNs are mainly divides into five-membered SNs and six-membered SNs. SNs usually undergo a dissociative equilibrium of two acid-base. At low pH 2–3, $–NH_2$ group protonates/deprotonates (pK_{a1}), while pH 5–7.5, a second protolytic dissociation (pK_{a2}) occurs at the $-SO_2$-NH-R group [26]. More precise physiochemical properties and structures are presented in Table 1.

2.1. Residues of sulfonamides in the environment

SNs have extensive antibacterial spectrum to Gram-positive bacteria and Gram-negative bacteria and they are also one of the most commonly used drugs in the fields of medical treatment, animal husbandry and veterinary medicine [33–35]. However, many environmental safety problems on SN residues have been reported. SN residues were frequently detected in water and sediment worldwide. This has aroused extensive attention. Fig. 1 describes the distribution of SNs in rivers and sediments. In Germany, the concentration of sulfamethazine (SMZ) was about 0.48 μg L^{-1} and 0.47 μg L^{-1} in river and groundwater, respectively [36]. Later, researchers observed that there were more than 10 kinds of SNs with the highest detection frequency in China, Spain, UK and other countries [37–40]. And the concentration of SNs was about 24–385 ng L^{-1} in the Haihe River Basin, China [41]. SNs concentration levels were 0.31–14.8 ng g^{-1} and 100 ng L^{-1}–100 ng g^{-1} in the Yangtze River sediments and the Yellow River sediments, respectively [12]. Other relevant data are illustrated in the Supporting Information.

Once entering the environment, SNs can be found in water, suspended substance, sediment, soil and biological substance. This is due to their migration, transformation and coordination. As shown in Fig. 2, human medicine, pharmaceutical wastewater, agriculture, livestock and aquaculture runoff are the main sources of SNs in the environment [48]. Surface runoff and leaching are their important transport routes. On the one hand, SN residues can interact with the soil system and put pressure on the natural microbial system. Microbial transformation may lead to metabolites re-transformation into the parent compounds [49]. On the other hand, SNs possess lower soil partition coefficient and stronger water solubility, and they are easier to enter groundwater with the leaching of rain water [50]. With the discharge of SNs industrial wastewater, human excretions containing SNs flow into the wastewater treatment plants through sewage pipeline. However, conventional wastewater treatment plant processes are not specifically designed to remove SNs, the parent molecule may be released directly into the receiving environment [14]. SNs eventually enter the surface water with the effluent from the wastewater treatment plants. SNs are also intensively used as herbicides in the field of agriculture, further absorbing by plants and accumulating in roots and leaves after spraying. These residues ultimately accumulated in the human body through the food chain, causing adverse effects on human health such as skin allergies, nausea and vomiting reactions [48].

2.2. Health and environmental effects of sulfonamides

SN residues have long time effects on the ecological environment and human beings, and its adverse effects cannot be ignored. SNs can not only reduce the biomass of microorganisms, but also affect the relationship between bacteria and fungi, thus causing changes in microbial diversity [51–53]. The changes of microbial diversity may directly affect the ecosystem [54]. Yang et al. [55] demonstrated that SNs have an acute toxic effect on *Photobacterium phophoreum*. And the sequence original solution acute toxicity was as follows: sulfachloropyridazine (SCP) > sulfadimethoxine (SDM) > sulfamerazine (SMR) > sulfadiazine (SDZ). Spraying SMZ with a certain concentration has partially inhibitory effects on the growth of roots and shoots [56,57]. For the lettuce, cucumber, tomato and carrot, the inhibitory rates of shoot elongation were 53.2%, 17.8%, 6.75%, and 9.42%, respectively, while the roots elongation reached 70.7%, 48.2%, 42.1%, and 32.7%, respectively [56]. In the application process, non-target organisms in the environment will inevitably be exposed to SNs and their derivatives. In addition, SNs may have synergistic effects with other pollutants, resulting in more adverse effects [1,56,58]. All of these factors may pose a potential ecological threat for the whole ecosystem. Therefore, the effort should not only reduce the amount of SNs in the environment, but also reduce the usage of SNs, and further investigate the chronic, acute toxicology of SNs and their derivatives. The following contents mainly introduce the major techniques (adsorption and AOPs) of SNs removal and the strengthening methods over the last decade to guide engineering applications.

3. Adsorptive removal of sulfonamides

3.1. Pyrogenic carbonaceous materials

Pyrogenic carbonaceous material (PCM) with polyaromatic sheet refers to the solid pyrolysis products of fresh or petrochemical biomass. Except for fossil, fuel soot [59,60], engineering carbon materials such as biochar (BC), activate carbon (AC), graphene (GE), graphene oxide (GO) and carbon nanotube (CNT) belong to PCM [21]. These carbonaceous materials have a strong affinity to pollutants due to their porous structure, large surface area and tunable surface functionality [61]. Therefore, it is widely used to remove pollutants from water. The following four sections mainly discuss the applications of the four engineering carbons. Table 2 presents the applications of the four engineering carbons (BC, AC, GE and CNT) in removing SNs.

Table 1
The main physiochemical properties and structure of SNs.

Molecular structure	Name	CAS number	Molecular formula	R	$LogK_{ow}$	Pk_{a1}	Pk_{a2}	Solubility (g L^{-1})	Ref.
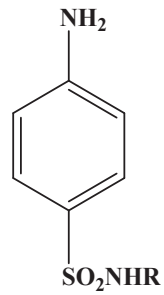	SMX	723–46-6	$C_{10}H_{11}N_3O_3S$	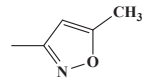	0.89	1.7	5.6	0.61	[16]
	SMZ	57–68-1	$C_{12}H_{15}N_4O_2S$	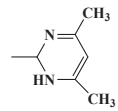	0.14	2.28	7.42	1.5	[27]
	STZ	72–14-0	$C_9H_9N_3O_2S_2$	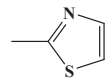	0.05	2.19	7.24	0.373	[28]
	SFZ	144–82-1	$C_9H_{10}N_4O_2S_2$	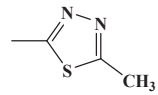	0.54	1.86	5.29	–	[29]
	SPD	144–83-2	$C_{11}H_{11}N_3O_2S$	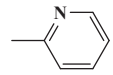	0.35	2.9	8.54	0.25	[27]
	SDZ	68–35-9	$C_{10}H_{10}N_4O_2S$	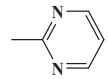	−0.34	2	6.48	0.067	[27]
	SSX	127–69-5	$C_{11}H_{13}N_3O_3S$	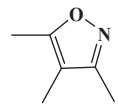	1.01	1.52	4.83	–	[30]
	SCP	201–269-9	$C_{10}H_9N_4O_2SCl$	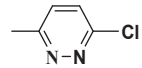	0.31	1.36	5.90	–	[30]
	SMR	127–79-7	$C_{11}H_{12}N_4O_2S$	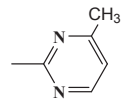	0.44	2.06	6.90	0.02	[31]
	SDM	122–11-2	$C_{12}H_{14}N_4O_4S$	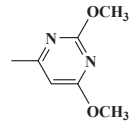	1.66	1.30	6.21	0.343	[32]

- Not Found.

3.1.1. Biochar-based materials

Low-cost BC, a carbon-rich product produced from waste biomass under anoxic conditions at below 800 °C [80,81], has drawn great attention in recent years due to unique features such as functional groups, porous structure and mineral components [28,82,83]. Rajapaksha et al. [62] investigated the effect of pyrolysis temperature on BC to remove SMZ. The results showed that BC produced at 700°C (TWBC-700) had a larger surface area (342.22 m^2 g^{-1}), more pore volumes (0.0219 cm^3 g^{-1}) and a higher aromatic degree compared with BC produced at 300 °C (TWBC-300). Meanwhile, they found that steam activation further increased the surface area (576.09 m^2 g^{-1}) and pore volume (0.1091 cm^3 g^{-1}) of higher temperature BC (TWBC-700S). The adsorption affinities followed the order of: TWBC-700S (0.1049 mmol g^{-1}) > TWBC-700 (0.0258 mmol g^{-1}) > TWBC-300 (0.0095 mmol g^{-1}) [62]. Besides, Sun et al. [84] investigated the effect of BC porosity on the adsorption capacity. They used organic acids (citric and malic acids) to modify the crop-straw-derived BC, leading to the release of the dissolved organic residues of BC. Experimental results showed that BC with higher porosity possessed better adsorption capacity for SMX [84]. It indicates that direct surface interaction and pore filling play a vital role in the adsorption of SNs by BC.

Nowadays, numerous modified BCs were gradually used to remove SNs. For example, biochar-coated multi-walled carbon nanotube (BC-MWCNT) was synthesized by dip-coating process and slow pyrolysis (300 °C and 600 °C) [85]. The results indicated that BC combined with carboxyl functionalized MWCNT greatly enhanced the physiochemical properties of BC (e.g., surface area, pore volume and functional groups). BC-MWCNT still had good reusability after five cycles and exhibited a high sorption capacity (0.1175 mmol g^{-1}) for SMZ. Subsequently, our group synthesized graphene oxide-coated biochar nanocomposites (GO-BC) to remove SMZ from aqueous solution [86]. The carboxyl groups, lactone groups and surface area of the nanocomposites were increased with the introduction of GO. The sorption capacity of GO-BC to SMZ increased by 1.14 times compared with original BC. Thus, BC combined with other carbon nanomaterials may enhance the adsorption performance of BC to SNs.

3.1.2. Activated carbon-based materials

AC is prepared by pyrolysis of waste and by-products under little or no oxygen conditions at above 900 °C and followed by "activation" process with gases or reagents [59]. Compared with BC, the production of AC requires a higher temperature and extra activation process [87]. BC is regarded as a sustainable and low-cost precursor of AC [88]. However, the application of no-activated BC is limited due to its low pore volume and surface area as well as limited functionality [89]. Over the past few years, tremendous research efforts have been devoted to develop physical activation and chemical activation techniques with the aim of overcoming the above disadvantages [90,91].

Previous studies have shown that the properties of AC (e.g., functionality, porosity, surface physical morphology and chemistry) vary

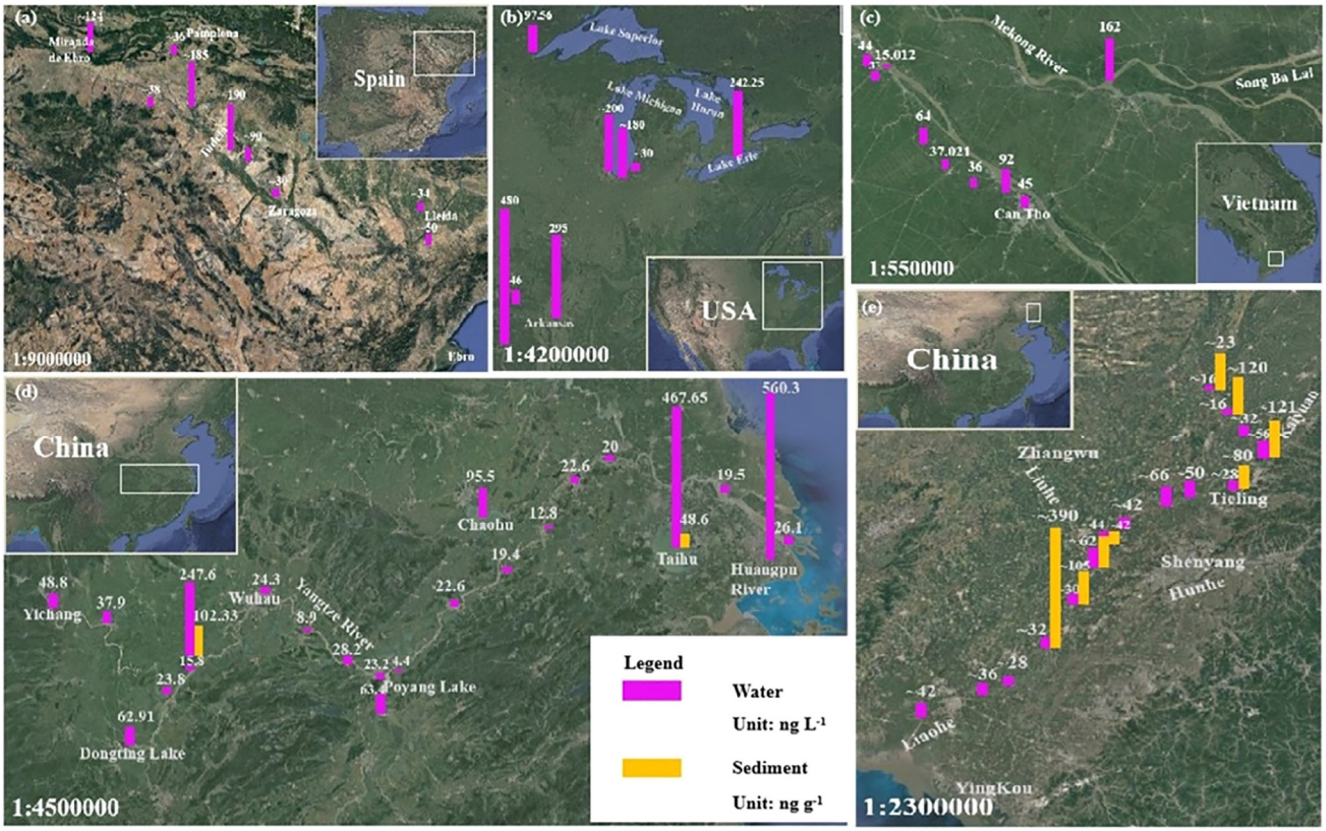

Fig. 1. The distribution of total SNs in rivers and sediments. (a) Ebro River basin, (b) Lake Erie, Southern Lake Michigan, Skaneateles Lake and Arkansas surface water, (c) Mekong River, (d) Yangtze River basin, (e) Liaohe River. The column chart represents the general distribution of the total concentration of SNs in water and sediments, respectively. The height of the column chart represents the level of total SNs concentration. The numerical data are from [11,40,42–47].

with raw material property and activation method [28,31]. And these properties play a vital role in the adsorption process. For example, Tonucci et al. [92] applied three types of powdered activated carbon (PAC) activated by stream to investigate SMX adsorption behavior: PAC-I, PAC-II, PAC-III (pinus tree, mineral carbon and coconut shell as precursor, respectively). The highest SMX adsorption (0.5178 mmol g^{-1}) was observed on PAC-I (pH 7.0, 25 °C and contact 2 h) due to its large mesopores and micropores volumes, indicating that large mesopores/micropores volumes played an important role in the adsorption process. In addition to extensive physical adsorption, surface reactions, internal transformation reactions in the pore system also take place during adsorption, which called reactive adsorption [93]. Liu et al. [69] reported that the introduction of Fe^{3+} ion could not only elevate the oxygenic functional groups on the AC surface and increase the polarity of AC, but also make Fe^{3+} on the AC surface coordinate with the amino group, further improving the adsorption capacity of SMZ.

3.1.3. Graphene-based materials

GE consists of a single layer of carbon atoms arranged into a hexagonal honeycomb structure with a sp^2-bond, which is regarded as the thinnest substance [28]. GE is a promising adsorbent due to its abundant electrons, easy modification with functional groups and combination with various functional materials [73,94]. For example, the adsorption capacity of SMZ on GE reached 0.3773 mmol g^{-1} at 45 °C [95]. In addition, Chen et al. [71] investigated the adsorption behaviors of functional GE (–NH_2, –COOH and –OH modified GE) and pristine GE on SMX in aqueous solution. The sorption capacity followed the order of: GE-OH (0.0455 mmol g^{-1}) < GE-COOH (0.0810 mmol g^{-1}) < GE-NH_2 (0.1605 mmol g^{-1}) < pristine GE (0.9447 mmol g^{-1}). This is because the flake graphite structure was destroyed by chemical reduction, functionalization and sonication during the preparation of functionalized graphene, further decreasing functionalized GE π-π interaction sites [71,96]. Therefore, their sorption capacities were significantly reduced.

Furthermore, GO is an important derivate of GE, which has unique properties and a highly reactive surface. GO is prepared by modifying GE with oxygen-containing functional groups [28]. Abundant oxygen-containing functional groups on the GO surface make it highly hydrophilic. GO is an excellent adsorbent for SNs removal, especially in aqueous environments. Chen et al. [97] studied the adsorption behavior of SMX on singer-layer GO in aqueous solution. The adsorption capacity reached 0.9486 mmol g^{-1} (pH = 5.0) because of the stronger π donor–acceptor interaction between SMX and GO. However, the adsorption of SMX on GO was inhibited when SMX and carbamazepine were co-adsorbed [98]. This is because carbamazepine with GO formed stronger π donor–acceptor interaction, thus reducing SMX adsorption capacity. Similarly, Song et al. [99] found that the Q_{max} of tetracycline and SMZ on reduced graphene oxide (rGO) in multi-component systems (0.5560 mmol g^{-1} and 0.4431 mmol g^{-1}, respectively) was lower than that of single system (0.7881 mmol g^{-1} and 0.6274 mmol g^{-1}, respectively), which was attributed to the competition of reactive sites [99].

However, GE is an ultralight material, so it is usually difficult to extract from suspensions. Thus, magnetic GE composite materials have become a hot research topic. According to the literature [100], magnetic rGO (Fe_3O_4-GO) composites were prepared by solvothermal reaction. As seen in Fig. 3, the loading of iron ions and the reduction of GO were carried out simultaneously in the presence of hydrazine hydrate (90 °C, pH 10). Besides, Fe_3O_4-GO can be effectively separated from water using magnet [100]. And Fe_3O_4-GO can be modified with porphyrin to prevent aggregation and expand its application [101].

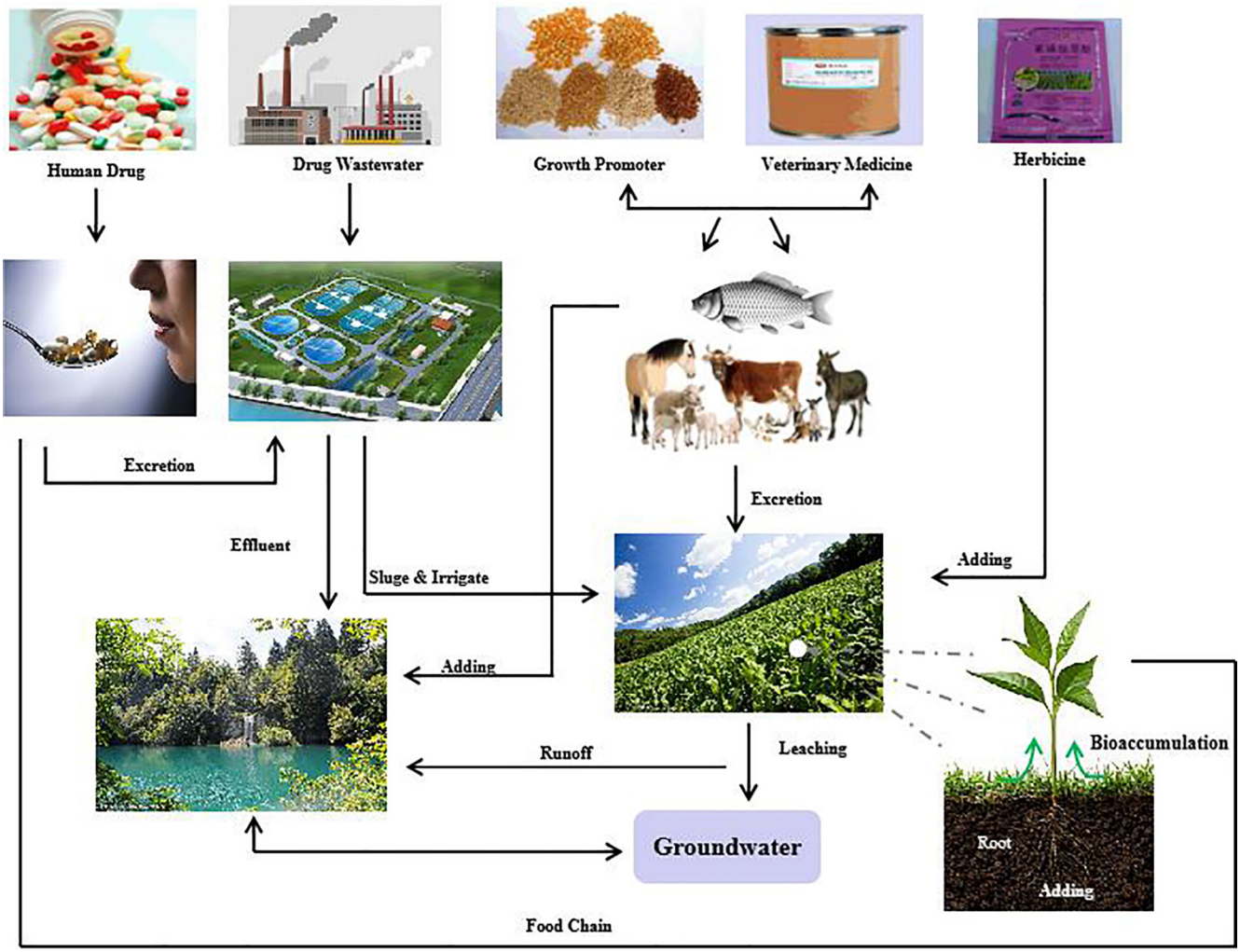

Fig. 2. Possible sources and transference processes of SNs in the environment.

3.1.4. Carbon nanotube-based materials

Although GE and CNT are carbon-based nanomaterials, their properties (dispersion vs. aggregation), dimensions (1D vs. 2D) and shape (planar vs. tubular) are highly different. CNT, both single and multi-wall, has cylindrical layered graphite sheets with a typical diameter distribution. The cylindrical structure of CNT provides massive conjunct sites that can be easily modified, which has attracted wide attention [102]. For example, CNTs-C/$CoFe_2O_4$ and CNTs-N/$CoFe_2O_4$ were used as adsorbents to remove SMX [74]. The CNTs/$CoFe_2O_4$ nanoparticles represented a potential alternative for the removal of micropollutants from aqueous solutions. And Table 2 presents the application of carbon nanotubes-based materials in removing SNs.

Furthermore, Wang et al. [103] studied the effect of oxidation process on adsorption performance of CNT. Oxidized CNT exhibited more oxygen-containing functional groups, which reduced the hydrophobicity of CNT and π-π interaction between CNTs and SMX. Thereby, the adsorption capacity was decreased. Wei et al. [104] further investigated the influences of the oxidation degree, functional group type and its loading position on the adsorption. As illustrated in Fig. 4a and b, the CNTs surface became more rough and defective after oxidation. The hydrophobicity of CNTs followed the order of MP > M10 > M30 > M50 (CNTs oxidized by 50% (w/w) HNO_3 solution), and M50 presented the lowest adsorption capacity for the four SNs (SDM, SFZ, SMZ, SMX). As shown in Fig. 4d, f, h and j, the structure of CNTs was damaged with the introduction of functional groups on the basal plane (B*) of CNTs [104]. Consequently, if the adsorption reaction occurs at the B* site of CNTs, π-π interaction could not form. For SNs adsorption occurred at the edge (E*) of CNTs (Fig. 4e, g, i and k), π-π interaction only weakened as the major structure of CNTs was not destroyed. According to DFT calculations, different functional groups have different degree of inhibition and followed the order of: $–COO^-$ > -C = O > –OH > –COC- [104], which was in well accordance with previous research results [32].

3.2. Metal-organic framework materials

MOF consisting of organic ligands and inorganic metal ions or metal clusters is considered as a new class of adsorbents of 21st century [105]. Owing to their unique features such as well-ordered porous structure, ultra-high surface area, versatile functionality and specific interaction sites, MOF has great potential to solve water pollution problems [106,107]. The complexation of MOFs with different metal nodes (e.g., Cr, Al, Fe, Co) has different properties, which has an important influence on its adsorption properties.

For example, Cychosz et al. [108] adopted two MOFs (HKUST-1 (a copper based MOF) and MIL-100 (Cr)) to remove sulfasalazine (SSZ) from aqueous solution. They found that MIL-100 (Cr) with trinuclear chromium clusters presented a larger adsorption capacity due to its good water stability. Gao et al. [78] further investigated the adsorption behaviors of SMX onto MIL-53(Fe), MIL-53(Cr) and MIL-53(Al). The adsorption capacity followed the order of: MIL-53(Fe) (0.314 mmol g^{-1}) < MIL-53(Al) (1.78 mmol g^{-1}) < MIL-53(Cr)

Table 2
Removal of SNs by using various adsorbents.

Adsorbent	SNs	Preparation	Surface area (m^2 g^{-1})	Reaction conditions	Performance	Mechanisms	Ref.
BC (AC)-based materials	SMZ	Tea waste was pyrolyzed at 700 °C for 3 h in N_2 atmosphere, then the pyrolysis samples were activated by steam for 45 min.	421.31 (raw BC), 576.09 (steam activation BC)	$[BC]_0$ = 1 g L^{-1}, $[SMZ]_0$ = 50 mg L^{-1}, contact time = 3 days, pH 3, T = 25 °C.	Q_{max}: 0.1216 mmol g^{-1}. Steam activation could effectively increase the surface area of BC.	π-π EDA, cation-π and cation exchange.	[62]
	SMX	Alfalfa was pyrolyzed at 650 °C for 2 h by heating 10 °C/min in N_2 atmosphere.	405	$[BC]_0$ = 0.2 g L^{-1}, $[SMX]_0$ = 100 mg L^{-1}, contact time = 7 days, pH 3.	Q_{max}: 0.3913 mmol g^{-1}. High temperature BC has higher surface area and the degree of carbonization.	Hydrophobic and π-π interaction	[63]
	SMZ SMX STZ	Wood was pyrolyzed at 400 °C for 2 h by heating 11 °C/min in N_2 atmosphere. Then the BC was soaked for 3 h at 50 °C in *ortho*-phosphoric acid, further pyrolyzing at 600 °C for 2 h.		$[BC]_0$ = 80 mg L^{-1}, [mix solutions]$_0$ = 20 mg L^{-1}, pH 4–4.25, contact time = 42 h, T = 25 °C.	Q_{max}: 0.0392 mmol g^{-1} (SMZ), 0.0482 mmol g^{-1} (SMX), 0.0522 mmol g^{-1} (STZ). Sorption affinity followed the order: STZ > SMX > SMZ.	H-bonding and EDA interaction.	[64]
	SMR	Cassava waste was pyrolyzed at 500 °C for 1 h by heating 10 °C/min. Then 50 g of BC was soaked in 1L 2 M KOH solution for 4 h at 25 °C and dried at 90 °C.	75.3 (raw BC), 128.42 (KOH-modified BC)	$[BC]_0$ = 10 g L^{-1}, $[SMR]_0$ = 30 mg L^{-1}, contact time = 48 h, T = 25 °C.	Q_{max}: 0.0025 mmol g^{-1}. KOH-modification slightly reduced the sorption capacity of BC for SMR.	Electrostatic and EDA interaction.	[65]
	SMR	Burcucumber plant was pyrolyzed at 700 °C for 3 h in limited air atmosphere, then the pyrolysis samples were activated by steam for 45 min.	2.31 (raw BC), 7.10, (steam activation BC)	$[BC]_0$ = 1 g L^{-1}, $[SMR]_0$ = 50 mg L^{-1}, contact time = 72 h, T = 25 °C. pH 3.	Q_{max}: 0.0779 mmol g^{-1} (raw BC), 0.1429 mmol g^{-1} (steam activation BC). Steam activation BC could effectively increase the adsorption capacity.		[66]
	SMX	The initial carbon was pyrolyzed at 800 °C under H_2S or N_2 atmosphere.	1541 (N_2), 1469 (H_2S)	$[BC]_0$ = 0.5 g L^{-1}, $[SMX]_0$ = 400 mg L^{-1}, contact time = 48 h, T = 25 °C, pH 3.	Q_{max}: 0.4348 mmol g^{-1} (H_2S), 1.0672 mmol g^{-1} (N_2).	Hydrophobic interactions.	[67]
	SMX	0.5 g of AC was soaked in 50 mL 50 mM $FeSO_4 \cdot 7H_2O$ solution and stirred for 0.5 h, then added ammonia. Finally the mixture with 1.5 mL 0.25 M $KMnO_4$ was treated by hydrothermal method (150 °C 12 h).	652	[Magnetic AC]$_0$ = 0.1 g L^{-1}, $[SMX]_0$ = 1 mg L^{-1}, contact time = 4 h, T = 25 °C, pH 7.	Q_{max}: 0.6285 mmol g^{-1}. Magnetic AC has good regeneration efficiency.	Hydrophobic, π-π and H-bonding interactions.	[68]
	SMZ	10 g of AC was soaked in 100 mL 0.75 M $FeCl_3$ solution for 24 h, then filter, cleaned and dried at 105 °C.	70.96 (AC), 166.23 (AC-Fe)	$[AC]_0$ = [AC-Fe]$_0$ = 6 g L^{-1}, [SMZ] = 100 mg L^{-1}, contact time = 48 h, T = 25 °C pH 7.	Q_{max}: 0.011 mmol g^{-1} (AC), 0.0620 mmol g^{-1} (AC-Fe). AC-Fe presented higher surface area, pore volume and functional groups.	Micropore capture, H-bonding and EDA interaction.	[69]
GE-based materials	SPD		7 (graphite), 331 (rGO1), 325 (rGO2)	$[SPD]_0$ = 50 mg L^{-1}, contact time = 7 days, pH 5, T = 25 °C.	Q_{max}: 0.5542 mmol g^{-1} (rGO_1), 0.4699 mmol g^{-1} (rGO_2), 0.0245 mmol g^{-1} (Graphite). SN^0 has great contribution to the total adsorption process.	Hydrophobic, EDA and electrostatic interaction.	[70]
	SMX			$[SMX]_0$ = 50 mg L^{-1} contact time = 24 h, pH 2–9	Q_{max}: 0.9447 mmol g^{-1} (GE), 0.1605 mmol g^{-1}(GE-NH_2), 0.0455 mmol g^{-1} (GE-OH), 0.0810 mmol g^{-1} (GE-COOH).	EDA and columbic interaction.	[71]
	SMX			$[GO]_0$ = 100 mg L^{-1}, $[SMX]_0$ = 10 μM, contact time = 24 h, pH 7, T = 25 °C.	Removal percentage: 12% (GO), 30% (GO combined with sonication). Sonication could enhance the sorption capacity of GO for SMX.	Hydrophobic and EDA interaction.	[72]
	SMZ		271.10	$[GE]_0$ = 0.2 g L^{-1}, $[SMZ]_0$ = 45 μM, contact time = 24 h, pH 7, T = 45 °C.	Q_{max}: 0.3773 mmol g^{-1}. Higher temperatures (45 °C) favored the reaction, compared to (25 °C and 35 °C).	EDA interaction.	[73]
CNT-based materials	SMZ		167 (raw MCNTs), 185 (MCNTs-OH)	$[SMZ]_0$ = 20 mg L^{-1}, contact time = 72 h, pH 5, T = 25 °C.	Q_{max}: 0.0877 mmol g^{-1} (raw MCNTs), 0.0479 mmol g^{-1} (MCNTs-OH). Functional groups played a side effect on the adsorption.	Hydrophobic, electrostatic, and EDA interaction.	[23]
	SMX	CNTs-C or CNTs-N suspension was mixed with $Co(NO_3)_2 \cdot 6H_2O$ and $Fe(NO_3)3 \cdot 9H_2O$ solution, then added NaOH solution, finally kept at 220 °C for 12 h in reactor, then washed and dried.	132.0 (CNTs-C/$CoFe_2O_4$), 134.4 (CNTs-N/$CoFe_2O_4$)	[CNTs-C/$CoFe_2O_4$]$_0$ = [CNTs-N/$CoFe_2O_4$]$_0$ = 0.1 g L^{-1} $[SMX]_0$ = 2 mg L^{-1}, contact time = 720 min, pH 5.5, T = 25 °C.	Q_{max}: 0.0276 mmol g^{-1} (CNTs-C/$CoFe_2O_4$), 0.0294 mmol g^{-1} (CNTs-N/$CoFe_2O_4$). CNTs-N/$CoFe_2O_4$ presented good reusability and stability.	Hydrophobic and π-π interaction.	[74]
	SPD	CNTs suspension with 10 g of sugarcane bagasse and hickory chips were stirred for	336 (BC-SDBS-CNT)	[BC-SDBS-CNT]$_0$ = 2 g L^{-1}, $[SPD]_0$ = 20 mg L^{-1}, contact time = 24 h, pH 6.7.	Q_{max}: 0.0155 mmol g^{-}1.		[75]

(*continued on next page*)

Table 2 (*continued*)

Adsorbent	SNs	Preparation	Surface area (m^2 g^{-1})	Reaction conditions	Performance	Mechanisms	Ref.
		1 h, dried. Then pyrolyzed at 600 °C for 1 h in N_2 atmosphere.					
MOF-based materials	SCP	1.087 g of $Cu(NO_3)_2{\cdot}3H_2O$ or 0.525 g of benzene tricarboxylic acids was dissolved in each 15 mL ethanol. The two solutions were then transferred to autoclave and heated at 120 °C for 12 h. Finally, dried sample was immersed in methanol for 2 days, dried.	1700 (HKUST-1)	$[HKUST\text{-}1]_0$ = 100 mg L^{-1}, $[SCP]_0$ = 40 mg L^{-1}, contact time = 2 h, pH 3.5, T = 25 °C.	Q_{max}: 1.5208 mmol g^{-1}. Most SCP was removed within 15 min.	H-bonding, π-π and electrostatic interactions.	[76]
	SMX	48 mL 4 g of $Cr(NO_3)_3$ and 1.66 g H_2BDC were placed in polytetrafluoroethylene liner, then added 0.425 mL 60% HF. The mixtures were stirred for 15 min and sonized 30 min. Finally, transferred to autoclave and heated at 210 °C for 8 h.	2338.31 (MIL-101(Cr))	$[MIL\text{-}101(Cr)]_0$ = 0.1 g L^{-1}, $[SMX]_0$ = 10 mg L^{-1}, contact time = 140 min, pH 7, T = 35 °C.	Q_{max}: 0.7187 mmol g^{-1}. MIL-101(Cr) showed good stability.		[77]
	SMX	$Cr(NO_3)_3{\cdot}9H_2O$, or $Al(NO_3)_3{\cdot}9H_2O$, or $FeCl_3{\cdot}6H_2O$ was mixed with *p*-phthalic acid and N,N-dimethylforramide. The suspension was transferred into oven and heated at 220 °C for 72 h.	~ 500 MIL-53(Cr) MIL-53(Al) MIL-53(Fe)	$[MIL\text{-}53]_0$ = 0.1 g L^{-1}, $[SMX]_0$ = 0.11 mM, contact time = 24 h, pH 7, T = 25 °C.	Q_{max}: 1.85 mmol g^{-1} (MIL-53(Cr)), 1.78 mmol g^{-1} (MIL-53(Al)) and 0.314 mmol g^{-1}(MIL-53(Fe)). Adsorption equilibrium was rapidly achieved within 60 min.	H-bonding, EDA and electrostatic interactions.	[78]
	SCP	0.529 g of $ZrCl_4$ or 0.37 g of benzene tricarboxylic acids was dissolved in 15 mL each 30 mL N,N-dimethylforramide. The two solutions were then transferred to autoclave and heated at 120 °C for 24 h. Finally, dried sample was immersed in chloroform for 5 days, dried.	1155 (UiO-66)	$[UiO\text{-}66]_0$ = 0.1 g L^{-1}, $[SCP]_0$ = 45 mg L^{-1}, contact time = 2 h, pH 5.5, T = 25 °C.	Q_{max}: 1.4632 mmol g^{-1}. UiO-66 presented a high surface area and defect-free structure which can enhance the adsorption.	Hydrophobic, π-π and electrostatic interactions.	[79]

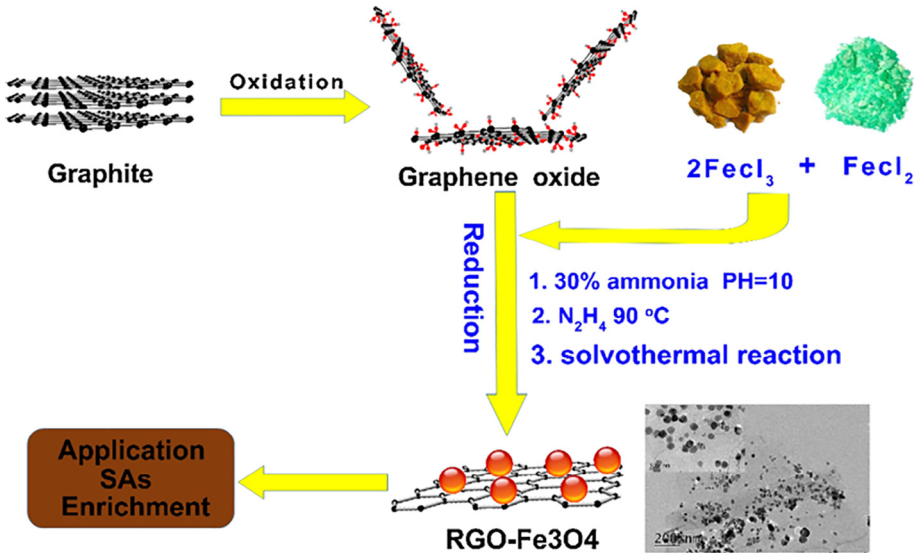

Fig. 3. Synthetic schematic for Fe_3O_4-GO. Reproduced with permission from Ref. [100]. Copyright 2016, Elsevier.

(1.85 mmol g^{-1}). As shown in Fig. 5b, narrow pore form (np) of MIL-53(Fe) hindered SMX to enter the internal channels and increased the binding energy. The sorption of SMX on MIL-53(Fe) relied only on electrostatic interaction. In contrast, MIL-53(Al) and MIL-53(Cr) exhibited large pore form (lp) and stronger H-bonding, electrostatic interaction, and π-π interaction (Fig. 5b), so they had higher adsorption capacity.

As shown in Table 2, there are various activated MOF materials used to remove SNs (In the preparation process, the solvent is not traditional water, but methanol, chloroform, etc.). For example, Azhar et al. [76] found methanol activated HKUST-1 (HKUST-1 immersed in methanol for 2 d) presented higher surface area and more unsaturated metal sites than that of HKUST-1, further increasing its adsorption capacity. After that, their groups [79] revealed that methanol activated ZIF-67 (ZIF-67-CH_3OH) exhibited higher surface area and larger average pore diameter than non-activated MOFs, but the adsorption amount of SCP on ZIF-67-CH_3OH had not improved significantly. This suggests that adsorption is not entirely dependent on the surface area and pore diameter of the adsorbent [79]. However, chloroform activated UiO-66 (UiO-66-$CHCl_3$) could remove most of SCP within 10 min. It was mainly due to the

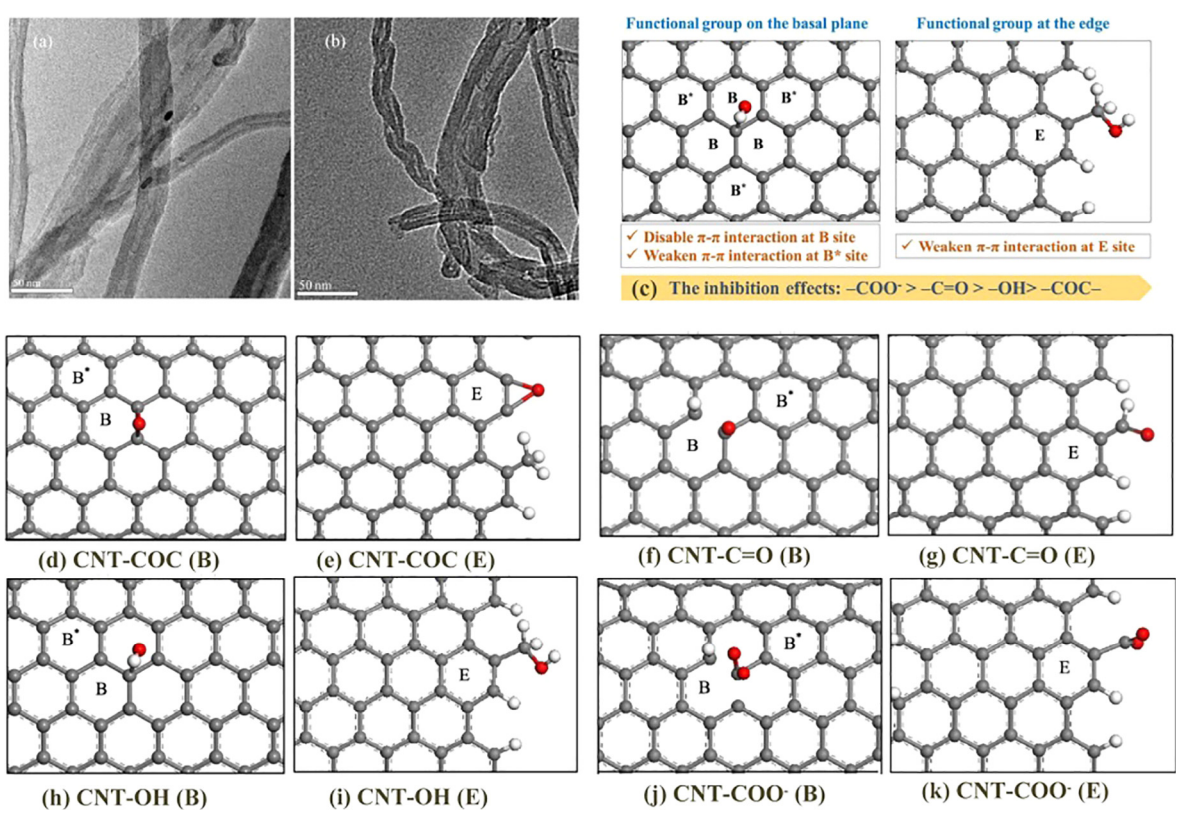

Fig. 4. TEM images of MP (a) and MP30 (b). (c) The effect of the position of functional groups on the adsorption (B* and E refer to the functional groups on the base and edge of CNTs, respectively). (d-k) Different positions of functional groups anchoring on CNT surface. Reproduced with permission from Ref. [104]. Copyright 2017, Elsevier.

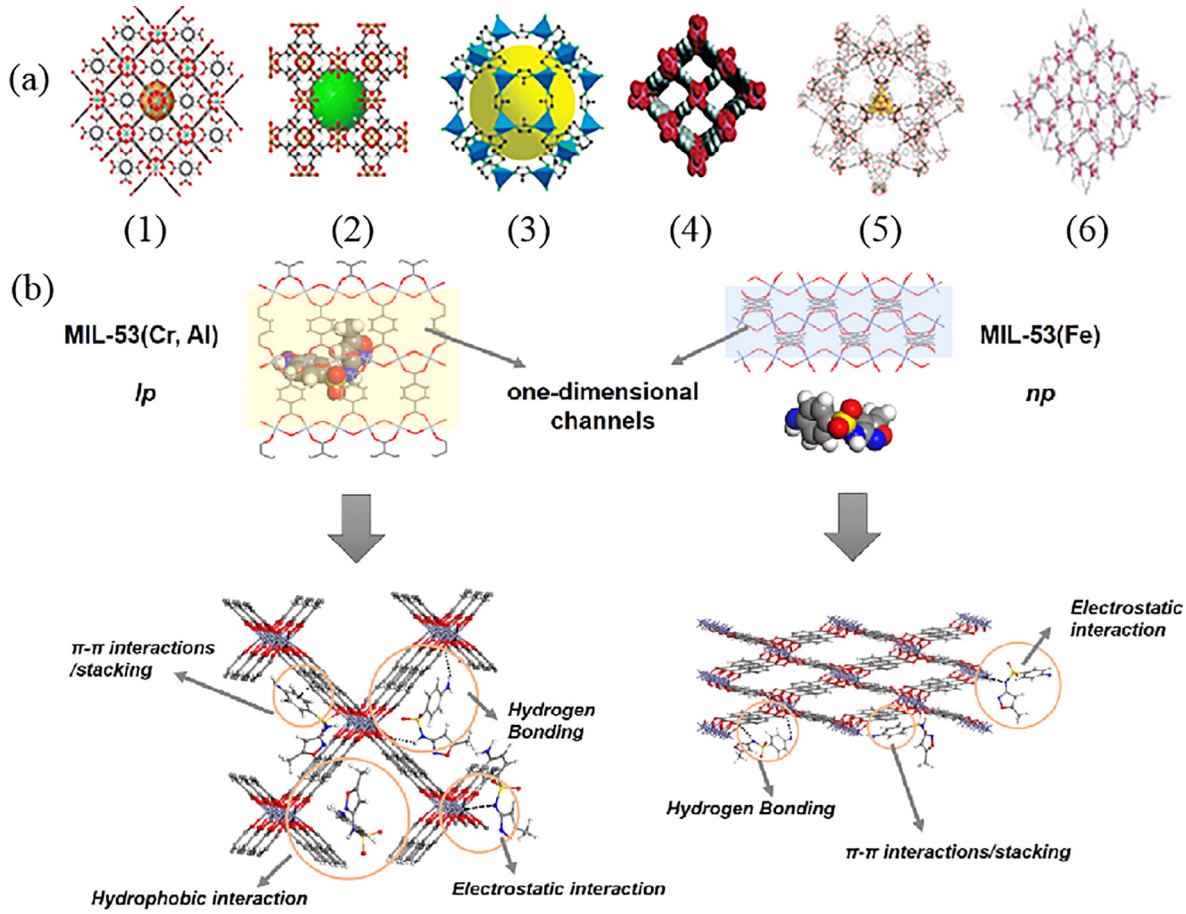

Fig. 5. (a) Structures of several typical MOFs. (1) UiO-66, (2) $Cu_3(BTC)_2$, (3) ZIF-8, (4) MIL-53, (5) MIL-101(Cr), (6) MOF-177. Reproduced with permission from Ref. [105]. Copyright 2016, Elsevier. (b) Adsorption mechanism of SMX on MIL-53(Cr), MIL-53(Al), and MIL-53(Fe). Reproduced with permission from Ref. [78]. Copyright 2019, Elsevier.

defect-free structure increased its hydrophobicity, sorption capacity and kinetics. And UiO-66-$CHCl_3$ still remained more than 80% removal efficiency after four recycles, indicating that it had good water stability [79]. Note that, MOF-derived nanoporous carbons (MOF was calcined at a high temperature) can also effectively remove SNs. The adsorption capacity of MOF-5-derived nanoporous carbons was up to 2.4704 mmol g^{-1} towards SMX in water phase [109]. The value was about 1.02–3.23 times higher than PAC and single-walled carbon nanotubes (SWCNT) under the same reaction condition. Ahmed et al. [110] observed that SMX sorption capacity of ZIF-8-derived nanoporous carbons produced at 1000 °C was 20 times higher than raw ZIF-8. It is anticipated that MOF-derived nanoporous carbon would be an excellent adsorbent for SNs removal from aqueous solution.

3.3. Other adsorbents

Many studies also reported the adsorption of SNs by soils [111–113], clay minerals (e.g., zeolite and bentonite etc.), and ion exchange resins [114–116]. For example, the expandable clay fractions of soil mineral exhibited strong affinity for SMX through ion exchange [114]. As fulvic acid-like substances exhibited a higher affinity toward SNs, soil treated with fulvic acid-like substances significantly expanded adsorption affinity for SMX and SPD [16]. Although SCP, SMX, SMZ and STZ cannot be effectively controlled in drinking water by ion exchange, SMX and SMZ can be efficiently removed by anionic resin (Lewatit MP500) [117]. The maximum adsorption capacities of SMX and SMZ were 1.0949 mmol g^{-1} and 0.0899 mmol g^{-1}, respectively. The adsorption mechanisms by magnetic ion exchange resin were mainly anion exchange and H-bonding [118]. Moreover, faujasite hydrophobic zeolite (zeolite Y) was used to remove SMZ, SDZ, and SCP [116]. Van der Waals type interactions and H-bonding were responsible for SNs extraction. The SNs were quickly ($t < 1$ min) removed from aqueous solution [116]. Martucci et al. [119] reported that zeolite Y with 200 silica/alumina ratio possessed a favorable kinetics. Furthermore, mordenite, HS zeolite mordenite, and ZSM-5 HS zeolites have been used to remove SNs [119,120].

4. Influences of environment conditions on adsorption

4.1. 1. Solution pH

SNs as amphoteric compounds have greatly pH-dependent in the adsorption process. Firstly, solution pH influences the distribution of SNs species (cation (SN^+), molecule (SN^0), and anion (SN^-)). Different SNs species exhibited different adsorption affinities [70]. As shown in Fig. 6a, SMZ^+ and SMZ^0 are the main species at pH < 3, while SNs mainly exist in the form of SN^- at pH > 6. Song et al. [99] proposed that the sorption distance of SMZ^0 on rGO (3.15 Å) was higher than that of SMZ^+ (1.83 Å) through density functional theory (DFT) calculation (Fig. 6b), indicating SMZ^+ state was more easily adsorbed by rGO. Secondly, the distributions of SNs species influence the adsorption mechanisms, further altering the adsorption capacity [79,95]. Thus, the value of solution pH is a critical factor regulating their adsorption [27,121].

As shown in Table 2 and Fig. 7, various adsorption mechanisms such as electron donor acceptor (EDA) interaction, charge assisted hydrogen

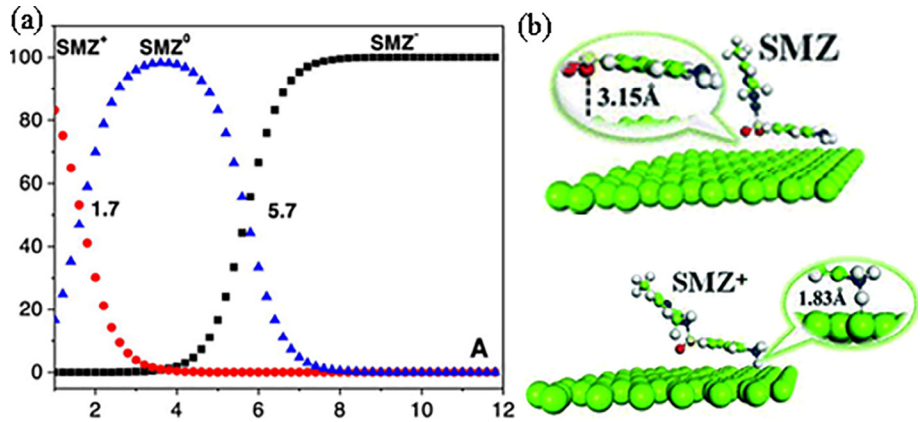

Fig. 6. (a) SMZ species distribution under the different pH conditions. Reproduced with permission from Ref. [122]. Copyright 2016, ACS. (b) Sorption distance of SMZ (neutral and protonated states) on rGO. Reproduced with permission from Ref. [99]. Copyright 2016, Royal Society of Chemistry.

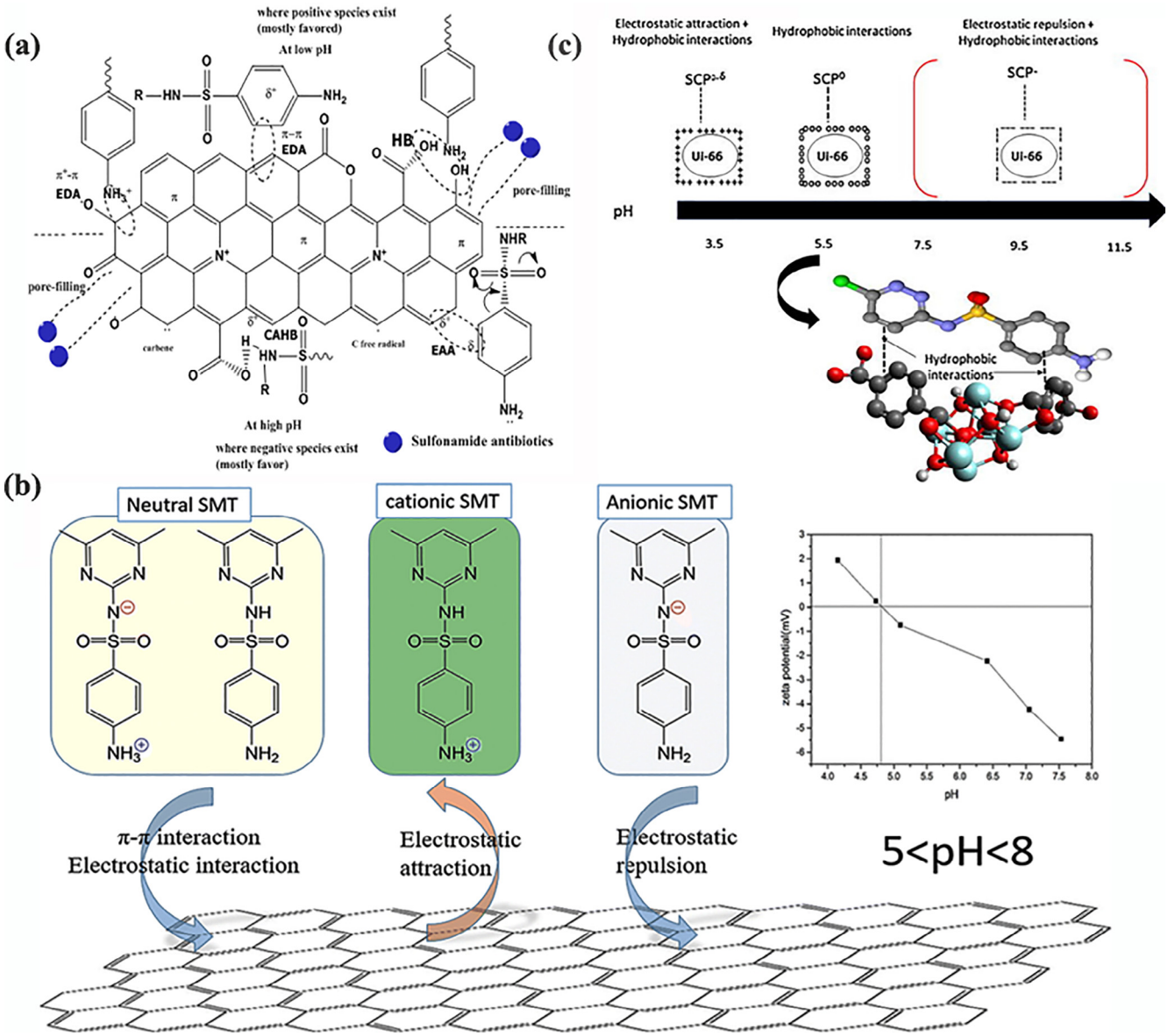

Fig. 7. (a) Adsorption mechanism of SNs on BC surface. Reproduced with permission from Ref. [33]. Copyright 2017, Elsevier. (b) Adsorption mechanism of SMT on GE at pH 5–8. Reproduced with permission from Ref. [95]. Copyright 2018, Springer. (c) Adsorption mechanism of SCP on UiO-66. Reproduced with permission from Ref. [79]. Copyright 2017, Elsevier.

bonding (CAHB) interaction, H-bonding, pore-filling, Van der Waals forces, Lewis acid-base interaction, electrostatic interaction and hydrophobic interaction were involved in SNs removal. However, these mechanisms may have different contribution proportions under different acid and base conditions [123]. At low pH, EDA interaction was regarded as the primary adsorption mechanism [72,124], which was attributed to the strong π accepting ability of SNs at low pH values. Besides, the highest sorption distribution coefficient (K_d) of SNs generally occurred at low pH values, SN^+ SN^0 was easily adsorbed [16,33,70]. When pH value was further increased to ~10, the solubility of SNs increased, and both SNs and adsorbent surfaces were negative, leading to an increase in hydrophilicity of SNs and in electrostatic repulsion, respectively [33,79]. Therefore, SNs adsorption amount will be significantly decreased at higher pH values. Yu et al. [32] found that the sorption of neutral species (SMZ^0, SMX^0, and STZ^0) on BC contributed the most to the total adsorption. The major mechanism was hydrophobic interaction for the pH-dependent SNs adsorption. Experimental results clearly revealed that hydrophobic interaction are the major adsorption mechanism rather than electrostatic interaction [32].

4.2. Matrix components

Owing to the existence of various matrix components (e.g., natural aquatic colloids, natural organic matter and various background ions) in real water, the adsorption behavior of SNs becomes more complicated. These matrix components may influence the adsorption mechanisms and thus alter SNs adsorption. As shown in Fig. 8, CNT existed inhibition effect on the sorption of SMX in the presence of inorganic nanoparticles (SiO_2 and Al_2O_3) [125]. For SiO_2, the inhibition effect enhanced with its rising particle size. By contrast, the adsorption amount of SMX was not obvious with the change of Al_2O_3 particle size. The results indicated that the inhibition effects depended on the dimension and type of the nanoparticles [125].

There existed inhibition effect for the adsorption of SNs on BC in the presence of bicarbonate, because bicarbonate can interact with BC surface through CAHB and compete with -SO_2NH- group for BC sorption sites. Adding other anions (such as Cl^-, CO_3^{2-}, SO_4^{2-} and PO_4^{3-}) slightly decreased the adsorption of SMZ on MWCNTs [23]. Besides, the presence of metal cations presented inhibition effects on SNs adsorption. For example, Cu^{2+} had a negative effect on adsorption of SNs on pine wood derived BC [22]. This is probably due to the form of complex internal structures between Cu^{2+} ions and oxygen-containing functional groups on BC surface. And Cu^{2+} was surrounded by hydrated structures that make it hard to form H-bonds [61]. Inyang et al. [75] found that no significant change in the sorption capacities of SPD on nanotube modified BC in the presence of Pb^{2+} ions, suggesting insignificant competitive effect of sorption sites between SPD and Pb^{2+}. Interestingly, both humic acid (HA) and Cr^{6+} could reduce the adsorption efficiency of SMX, whereas Cd^{2+} could promote the adsorption efficiency [126].

5. Reactive removal of sulfonamides

To date, extensive works have been conducted to degrade SNs [127]. As a special class of deep oxidation technology, AOPs with excellent degradation efficiency have become a hot spot in field of treatment research [128]. AOPs involve the in-situ generation of reactive radicals (e.g., •OH, $SO_4^{\bullet-}$, $O_2^{\bullet-}$ etc.). Especially •OH and $SO_4^{\bullet-}$ radicals, they are highly reactive species with higher reaction rate constants (10^6 to 10^9 M^{-1} s^{-1}). Therefore, it is possible to mineralize or oxidize the targeted compounds into low toxicity or non-toxic small molecules. UV-photolysis, photocatalytic process and Fenton/Fenton-like process are the most commonly used techniques for SNs removal among AOPs. The main purpose of this section is to study the degradation efficiency and mechanism of SNs in the different processes.

5.1. UV-photolysis

Photolysis as a natural attenuation process has been indicated to be the important degradation process of SNs [8]. In natural water, the half-life ($t_{1/2}$) of SMX was 5.4–7.8 h [129], while the $t_{1/2}$ was only 0.86 h in ultrapure, which can be explained in terms of SMX can complex with

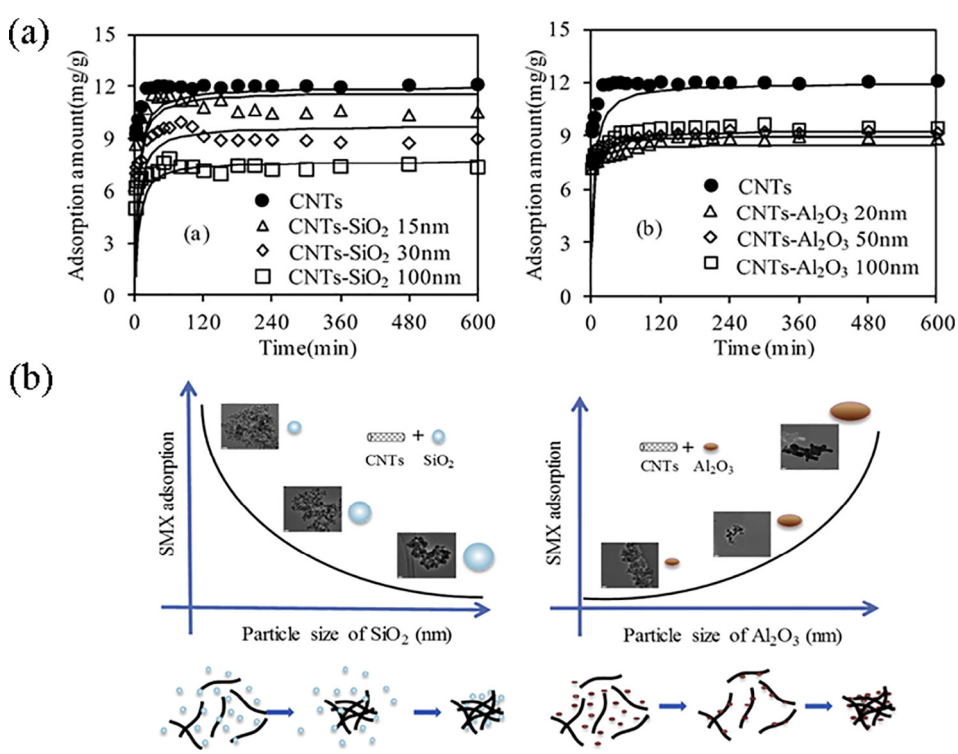

Fig. 8. (a) Adsorption kinetics of SMX on CNT in the absence and presence of SiO_2 (left) and Al_2O_3 (right). (b) Effect of size and the type nanoparticles for removal of SMX by CNT. Reproduced with permission from Ref. [125]. Copyright 2017, Elsevier.

cations or anions in water (e.g., Br^-, Cl^-) and consume •OH radicals [129]. And the direct photolysis rate of SNs is greatly dependent upon its the heterocyclic R group [130]. In general, six-membered SNs (e.g., SMZ, SDM, SDZ, SMR and SCP) presented a lower photodegradation rate than those five-membered SNs (e.g., SFZ, SMX, STZ and SSX) [30]. This is due to the heteroatoms (e.g., O, S and N) located in the five-membered SNs can provide their lone-pair, forming a delocalized π bond plane with the aromatic ring. This allows the five-membered SNs possess higher electron density. The higher electron density makes it have strong photon absorption ability [30,131]. Therefore, SNs with five-membered heterocyclic group are more likely to induce photodegradation reaction. Moreover, among SFZ, SMX, STZ and SSX, SMX and SSX presented higher degradation rates due to the O atom had stronger electronegativity than S atom and N atom [30].

In fact, only part of SNs can be direct photodegraded in wastewater (1–34%), drinking water (2–57%) and reclaimed water (5–81%) [30]. However, Yang et al. [132] found that whether pure water, surface water or ground water, the removal rate of SNs can be greatly improved when UV combined with hydrogen peroxide (H_2O_2) and peroxydisulfate (PDS). This is because both H_2O_2 and PDS can be cleaved into •OH (Eq. (1)) and $SO_4^{\bullet-}$ (Eq. (2)) under UV light, respectively. Ge at al. [133] conducted a detailed study on the photolysis behavior of five-membered SNs such as SMX, SSX, STZ and SFZ. As shown in Fig. 9, the cleavage of S-N bond was more likely to occur in direct photolysis compared with •OH-mediated indirect photolysis. H-abstraction and electrophilic C 1-attack were easier in •OH-mediated indirect photolysis. Besides, the two indirect pathways were also suitable for six-membered SNs (e.g., SDM) [133].

$$H_2O_2 + h\nu \rightarrow 2\cdot OH \quad (1)$$

$$S_2O_8^{2-} + h\nu \rightarrow 2SO_4^{\bullet-} \quad (2)$$

Furthermore, Wu et al. [29] found that the photodegradation rates of SDZ, SFZ, SMX and STZ were the highest in UV/PDS compared with UV/H_2O_2 and UV/$NaBrO_8$, which were 0.0245 min^{-1}, 0.0096 min^{-1}, 0.0283 min^{-1}, and 0.0141 min^{-1}, respectively. This is because both the reduction potential and reaction selectivity of $SO_4^{\bullet-}$ (2.5–3.1 V) [134] are higher than •OH (1.8–2.7 V) [135], and the quantum yield of PDS is larger than H_2O_2 in UV system at 254 nm (1.4 vs 1.0) [136,137]. The SNs oxidation by UV/PDS possesses the advantages of the wide operating pH range and the stability [132,138,139]. Similarly, Ji et al. [140] also found that UV/PDS (96.2%) appeared to be more efficiency than in UV/H_2O_2 system (93.1%) for SSZ degradation. And four intermediates are mainly produced by azo bond cleavage, SO_2 extrusion and smiles-rearrangement. In addition, UV/PDS had a better radical quantum yield than UV/H_2O_2 system, resulting in the faster degradation of SMX and trimethoprim (TMP) by UV/PDS [141]. Acosta-Rangel et al. [132] analyzed the degradation efficiency, by-products and toxicity of SMZ, SDZ and SFZ by UV, UV/H_2O_2 and UV/PDS. The degradation efficiency of SMZ reached nearly 100% with the addition of 0.44 mM H_2O_2 or PDS ($[SMZ]_0$ = 15 mg L^{-1}). As shown in Fig. 10, the degradation pathways

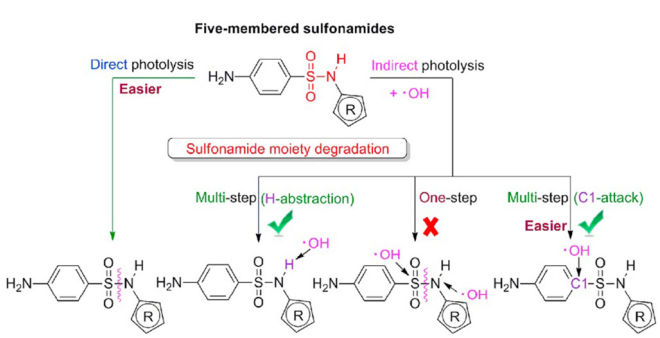

Fig. 9. Scheme of photolysis pathways for five-membered SNs in UV/H_2O_2 system. Reproduced with permission from Ref. [133]. Copyright 2018, Elsevier.

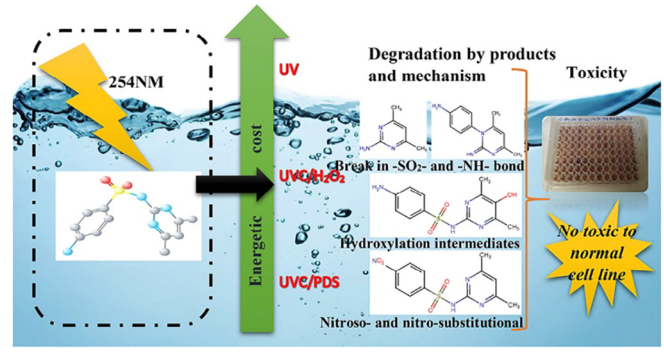

Fig. 10. (a) Scheme of the SMZ degradation intermediates, mechanisms and energy cost under UV, UV/H_2O_2, UV/PDS system. Reproduced with permission from Ref. [132]. Copyright 2018, Elsevier.

were different in UV (cleavage of N-S bond), UV/H_2O_2 (hydroxylation) and UV/PDS (electrophilic reaction) systems, resulting in the different intermediates. These intermediates were less cytotoxic than the parent compounds [132]. Moreover, UV/PDS energy consumption was lower due to SNs reacted more rapidly with $SO_4^{\bullet-}$.

5.2. Photocatalytic degradation

Recently, the application of photocatalysis has been investigated intensively among AOPs [142,143]. The process involves at least three steps: (i) catalyst is activated by light, (ii) photocarrier separation or transport, (iii) the reaction takes place on the photocatalytic surface [144]. This process is called "an accelerated light reaction under the presence of a catalyst" [145]. There are numerous catalysts (e.g., TiO_2, ZnO, WO_3, C_3N_4, CNT etc.) with good photocatalytic activity [146-151]. According to the composition of the photocatalyst, the paper divides the photocatalysis into the following two categories: metal-based photocatalysis and metal-free-based photocatalysis.

5.2.1. Metal-based photocatalysis

Metal-based catalysts (such as TiO_2, ZnO, WO_3, CuS, Fe_2O_3, BiO_mX_n (X = Cl, Br, and I) in single photocatalytic systems have attained wide attention. However, the applications of these photocatalysts at full-scale are still limited because of the rapid recombination of electron (e^-)-hole (h^+), inappropriate band values and positions and sluggish surface reaction kinetic [152,153]. Several strategies have been developed to optimize photocatalysts, including defect engineering, construction of homogeneous and heterogeneous junctions, and morphology control [24,154].

Nowadays, many remarkable results have been achieved. For example, the photocatalytic of Ag_3PO_4/WO_3 (75:25) composites (Ag_3PO_4:WO_3 molar ratios of 75:25) apparently higher than pure WO_3, as depicted in Fig. 11c [148]. Fig. 11b showed clear lattice fringes, suggesting the intimate contact between Ag_3PO_4 and WO_3, which may be more conducive to charge transfer. As shown in Fig. 11c-d, Ag_3PO_4/WO_3 (75:25) presented a higher degradation rate than TiO_2/WO_3 [148,155]. However, the reusability and stability of Ag_3PO_4/WO_3 composites were poor attributed to silver partially dissolved in aqueous phase and silver phosphate turned into metallic silver [148].

Another type of composite photocatalysts based on WO_3, one containing graphitic carbon nitride (WO_3-g-C_3N_4) [156] and the other holding CNTs (WO_3-CNT), [157] which were used to remove SMX under 300 W visible light irradiation. Under similar reaction conditions, the removal efficiency reached 76.7% within 4 h [156] and 73.3% within 3 h [157], respectively. As shown in Fig. 12a, b, there existed similar mechanisms: •OH and h^+, •OH and $O_2^{\bullet-}$ were the main contributors in the photocatalytic process. In brief, both g-C_3N_4 and CNT acted as electron traps, and remarkably enhanced e^--h^+ separation.

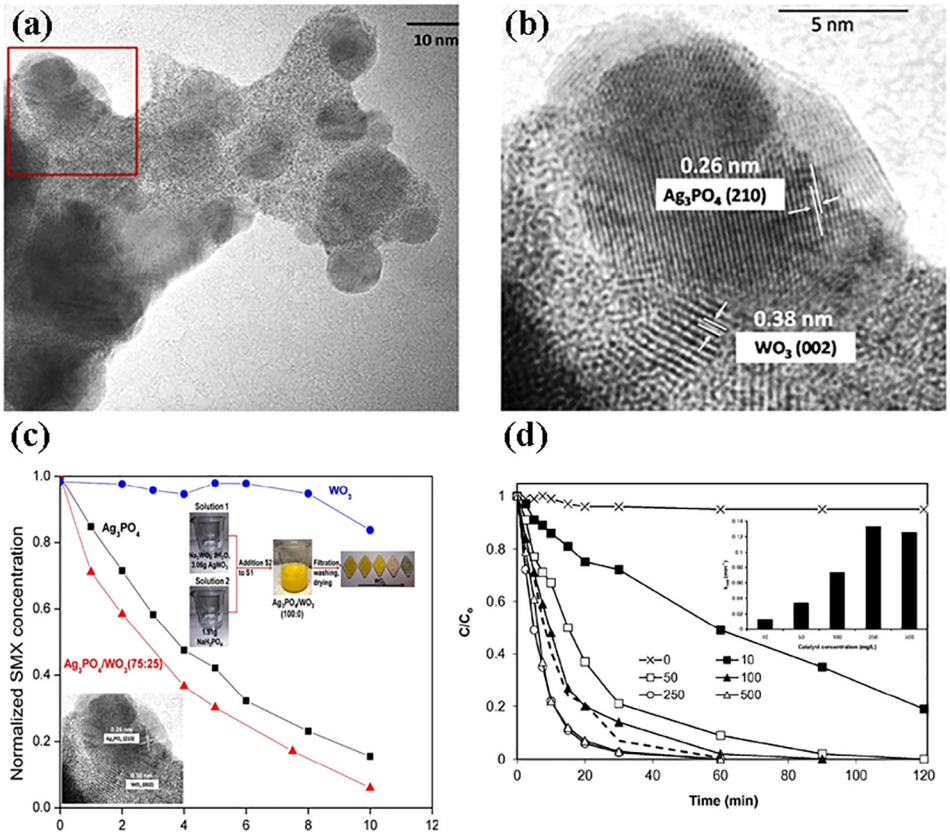

Fig. 11. HRTEM image (a) and a magnified view of Ag_3PO_4/WO_3(75:25) photocatalysts (b). (c) Photocatalytic performance of pure Ag_3PO_4, pure WO_3 and their composites for the degradation of SMX in ultrapure water ($[Ag_3PO_4/WO_3]_0$ = 100 mg L^{-1}, $[SMX]_0$ = 525 μg L^{-1}). Reproduced with permission from Ref. [148]. Copyright 2018, Elsevier. (d) The degradation of SMX on TiO_2/WO_3 with different doses in ultrapure water ($[SMX]_0$ = 350 μg L^{-1}). Reproduced with permission from Ref. [155]. Copyright 2017, Elsevier.

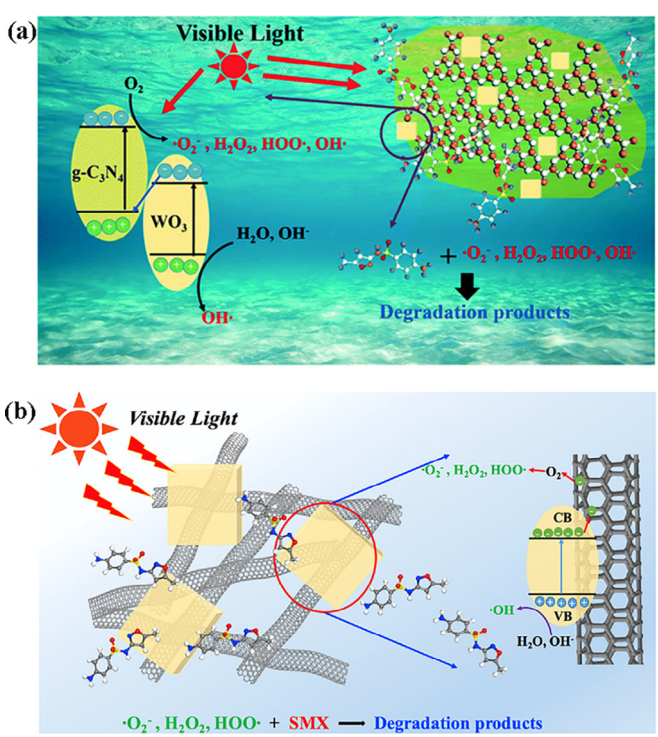

Fig. 12. (a) Degradation mechanism of SMX by WO_3-g-C_3N_4 under visible light irradiation. Reproduced with permission from Ref. [156]. Copyright 2017, Royal Society of Chemistry. (b) SMX degradation mechanism by WO_3-CNT under visible light irradiation. Reproduced with permission from Ref. [157]. Copyright 2018, Elsevier.

WO_3 combined with g-C_3N_4 or CNT greatly improved visible light harvesting ability of original WO_3, furthering its photocatalytic performance [156,157]. Besides, WO_3-g-C_3N_4 composites with large surface area were conducive to adsorption. The degradation of SNs with other metal-based photocatalysts is presented in Table 3.

5.2.2. Metal-free-based photocatalysis

Compared with metal-based catalysts, metal-free-based catalysts can overcome metal leaching problem in the degradation process, which are considered as environmentally friendly catalysts [158]. Among the numerous metal-free catalysts, g-C_3N_4 and BC have gained much attention due to their low-cost and easy preparation [159–163]. According to the literature [164], the removal percentage of SMZ on hyrochar reached 72% under daylight irradiation, which was 2 times higher than that of pyrochar. This is due to the more photoactive surface oxygen functional groups in hydrochar, the more reactive species (singlet oxygen ($^1O_2$), $O_2^{\bullet-}$, H_2O_2, •OH) could be generated under light [164]. Huang et al. [165] found that higher-temperature (800 °C) pyrochar showed good degradation performance for SMZ because of the better morphological features. Hence, the effects of pyrolysis temperature on the performance of the catalysts cannot be ignored when preparing carbon-based catalysts.

Nowadays, g-C_3N_4-based metal-free catalysts have also received widely attention due to its medium-bandgap (2.7 eV) and desirable visible-light response. Song et al. [166] studied the photodegradation behavior of SMX, SDZ, SSX and SMZ by g-C_3N_4. The removal efficiency of the four SNs exceeded 90% within 100 min under visible light irradiation (C_0 = 10 μM, [g-C_3N_4] = 50 mg L^{-1}). Besides, they found that the degradation pathways and major reactive species were different for different SNs. The results indicated that $O_2^{\bullet-}$, and h^+ acted as the dominant reactive species for SMX, SDZ and SMZ, while •OH and h^+ played a major role in the photodegradation of SSX [166]. For the degradation pathway, hydroxylation of the benzene ring and cleavage of S-N bond were the common degradation pathways of SMX, SSX, SDZ, and SMZ, which were also the main pathways for SSX. But carboxylation of methyl group and cleavage between benzene ring and S occurred

Table 3
Selected research studies on the applications of photocatalysis technologies to remove SNs.

Photocatalysts	SNs	Preparation method	Reaction conditions	Removal efficiency	Mechanism	Advantages or Disadvantages	Ref.
Metal-based catalysts	SMX	By deposition–precipitation method. $Na_2WO_4{\cdot}H_2O$ and NaH_2PO_4 were dissolved in each 25 mL water. Then the two solutions were added in 50 mL $AgNO_3$ solution. Finally, the mixtures were stirred at room temperature for 4 h.	$[Ag_3PO_4/WO_3]_0$ = 200 mg L^{-1}, $[SMX]_0$ = 525 μg L^{-1}, reaction time = 10 min, 100 W xenon lamp ($\lambda > 420$ nm).	90%	Reactive species: h^+ Degradation pathway: the cleavage of the S-N bond and isoxazole ring.	The activity of the catalyst decreased significantly after two cycles.	[148]
	SMX	By sol–gel method. Pretreated BC was dispersed in 60 mL ethanol and then added 20 mL $Ti(OCH(CH_3)_2)_4$. The mixtures were then stirred for 1 h and followed added 8 mL HCl and 20 mL ethanol, stirred for 1 h. Finally, the dried sample was heated at 325 °C for 1 h.	$[BC/TiO_2]_0$ = 5 g L^{-1}, $[SMX]_0$ = 10 mg L^{-1}, reaction time = 6 h, pH = 4, 15 UV lamp (λ = 254 nm).	91%	Reactive species: •OH $O_2^{\bullet-}$, and $CO_3^{\bullet-}$ radicals. Degradation pathway: hydroxylation and di-hydroxylation.	The system showed high SMX mineralization (81%) and accumulation of non-toxic products.	[147]
	SMX	By hydrothermal method. The prepared GO was dispersed in DI water and treated with ultrasound. Then $Na_2WO_4{\cdot}2H_2O$ and HCl were added in the mixed suspension, respectively. Finally, the suspension was transferred to autoclave and heated at 140 °C for 8 h.	$[rGO\text{-}WO_3]_0$ = 1 g L^{-1}, $[SMX]_0$ = 10 mg L^{-1}, reaction time = 3 h, no pH adjustment, 200 W Xe arc lamp (420 nm < λ < 630 nm).	98%	Reactive species: $O_2^{\bullet-}$ and •OH radicals. Degradation pathway: hydroxylation, the cleavage of the S-N bond, benzene ring and isoxazole ring.	The catalyst exhibited good photostability and recyclability and can be used for pratical application.	[168]
	SMZ	By sol-hydrothermal method. 10 mL tetra-butyl titanate and 5 mL glacial acetic acid were added in 40 mL anhydrous ethanol and stirred for 2 h. Next, 50 mL $Bi(NO_3)_3{\cdot}5H_2O$ and 0.5 g of PAC were added slowly to the mixture, respectively. Finally, the above mixture was stirred for 8 h and then heated at 150 °C for 12 h in a reactor.	$[Bi\text{-}Ti/PAC]_0$ = 1 g L^{-1}, $[SMZ]_0$ = 20 mg L^{-1}, reaction time = 300 min, pH = 6, 300 W Xe arc lamp (400 nm < λ < 780 nm).	81.18%	Reactive species: h^+, •OH and $O_2^{\bullet-}$ radicals. Degradation pathway: hydroxylation and the break of sulfanilamide bond.	The composites exhibited high surface area, small particle size and low band gap energy.	[169]
	SMZ	By deposition–precipitation method. Pretreated $Bi_{12}O_{17}Cl_2$ was dispersed in 50 m DI water and then added 0.17 g of $AgNO_3$. The mixture was stirred for 1 h. Finally, AgI was slowly added in the above mixture and stirred for 1 h to synthesize the composites.	$[AgI/Bi_{12}O_{17}Cl_2]_0$ = 1 g L^{-1}, $[SMZ]_0$ = 10 mg L^{-1}, reaction time = 60 min, 300 W Xe lamp with 420 nm cut filter.	96.15%	Reactive species: h^+ and $O_2^{\bullet-}$ radicals. Degradation pathway: Carboxylation; the decay of pyrimidine ring and the cleavage of the S-N bond.	The composites exhibited good recyclability.	[142]
	SMZ	By hydrothermal method. $Fe(NO_3)_3{\cdot}9H_2O$ and $Zn(NO_3)_2{\cdot}6H_2O$ were dissolved in 50 mL DI water and stirred for 30 min which was placed in Teflon-lined autoclave. Next, 0.5 g of g-C_3N_4 and 1.2 g of urea were added and then stirred for 1 h. Then, the mixture was kept at 120 °C for 24 h. Finally, the dried sample was heated for 3 h at 300 °C to synthesize the composites.	$[ZnO/Fe_2O_3/g\text{-}C_3N_4]_0$ = 0.5 g L^{-1}, $[SMZ]_0$ = 1 mg L^{-1}, reaction time = 480 min, natural pH, 500 W Xe lamp ($\lambda > 420$ nm).	~100%	Reactive species: $O_2^{\bullet-}$ and •OH radicals. Degradation pathway: hydroxylation, cleaving (S-N bond and C-S bond), oxidation, denitrification.	The composites still remained good recyclability and stability in 5th cycle.	[170]
Metal-free-based catalysts	SMZ	By wet chemistry/ thermal treatment. 10 g of urea with 2-thiobarbituric acid were mixed with 5 mL DI water and 5 mL ethanol to form H-bond interaction. Then the dried sample was placed in a crucible and heated for 2 h at 550 °C.	$[TCN]_0$ = 1 g L^{-1}, $[SMZ]_0$ = 10 mg L^{-1}, reaction time = 60 min, 300 W Xe lamp with a 420 nm filter.	97%	Reactive species: h^+ and $O_2^{\bullet-}$ radicals.	TCN presented high catalytic H_2 production activity.	[171]
	SMZ	By thermal treatment/wet chemistry. 10 g of urea and salicylic acid were mixed with 8 mL DI water and 2 mL ethanol. Then the suspension was stirred for 1 h and ultrasonicated for another 1 h. Finally, the dried sample was placed in a crucible and heated for 2 h at 550 °C.	$[CN\text{-}SA]_0$ = 0.5 g L^{-1}, $[SMZ]_0$ = 100 μM, 300 W Xe lamp ($\lambda > 420$ nm).	~ 99%	Reactive species: h^+ and $O_2^{\bullet-}$ radicals.	CN-SA exhibited good stability and photocatalytic activity after four cycles.	[167]
	SMZ	By hydrothermal and pyrolysis method. Hydrochar (HTC-F): wood powder was added in 50 m DI water and stirred for 2 h. Then poured into Teflon-lined autoclave and heated for 5 h at 200 °C. Pyrochar (PC-F): wood powder was placed in tube furnace and pyrolyzed at 450 °C for 3 h.	$[HTC\text{-}F]_0$ = $[PC\text{-}F]_0$ = 100 mg L^{-1}, $[SMZ]_0$ = 250 μg L^{-1}, reaction time = 6 days, daylight irradiation.	72% (HTC-F) 50% (PC-F)	Reactive species: •OH radicals.	Hydrochar could generation more H_2O_2 and •OH under daylight irradiation.	[164]

on SMZ and SSX, respectively [166]. It suggests that different active species may lead to different degradation pathways of SNs.

Nowadays, g-C_3N_4 composites were gradually used to remove SNs. For example, our groups investigated the photocatalytic activity of carbon nitride modified with barbituric acid (BCM-C_3N_4) and carbon nitride modified with salicylic acid (TCN) for SMZ. [34,167]. Compared with pure g-C_3N_4, both composites presented higher degradation rate for SMZ. This is because both barbituric acid and salicylic acid efficiently increased the charge carrier separation of g-C_3N_4 and improved visible light absorption. In addition, BCM-C_3N_4 exhibited a high surface area (179 $m^2 g^{-1}$) [34]. Through radical species trapping experiments, both $O_2^{\bullet -}$ and h^+ were the predominant radicals in these two photoreactive systems. Other related applications of metal-free-based catalysts are presented in Table 3.

5.3. Fenton/Fenton-like degradation

Fenton process is inorganic chemical reaction which is based on the generation of highly active •OH during the reaction of H_2O_2 and ferrous iron (Fe^{2+}) at pH of around 3 [173,173], and the formed Fe^{3+} can be easily reduced by H_2O_2, leading to the generation of HO_2• radicals. The formed •OH can oxidize organic pollutants. At present, many related researches have been conducted because the process is safe, fast, economic and environmental friendly [174,175]. Table 4 presents SNs removal examples by various Fenton processes. For example, Velásquez et al. [176] found that the amount of Fenton's reagent ($[Fe^{2+}] = 157\ \mu mol\ L^{-1}$, $[H_2O_2] = 1219\ \mu mol\ L^{-1}$) in photo-Fenton process was less than in Fenton process ($[Fe^{2+}] = 192\ \mu mol\ L^{-1}$, $[H_2O_2] = 1856\ \mu mol\ L^{-1}$) under the same reaction condition. The behavior is due to the presence of light promoted the conversion of Fe^{3+} to Fe^{2+}, enhancing the additional •OH generation. The reaction processes mentioned above were displayed in Fig. 13 [177]. Martinez-Costa et al. [177] also found photo-Fenton exhibited better performance for SMX and TMP removal than traditional Fenton process. In addition, the degradation kinetic of SMX and TMP by UV radiation was faster than by solar radiation (Fig. 13b, c). Taking advantages of high mineralization and low toxicity of by-product in solar photo-Fenton, using solar photo-Fenton is also a good alternative [177].

Even so, the practical applications of Fenton processes mentioned above are greatly limited by the limited pH range, large consumption of H_2O_2 and massive accumulation of iron sludge. Therefore, many researchers were beginning to focus on heterogeneous Fenton, combining it with ultrasound, electricity and light [178,179]. Heterogeneous Fenton catalysts such as iron minerals, copper ferrite and other iron-containing catalysts have attracted much attention [180-182]. For example, Barhoumi et al. [183] found that pyrite (FeS_2) presented a high catalyst activity towards SMZ in electro-Fenton system, in which plenty of H_2O_2 was produced. Furthermore, both 3D mesoporous $CuFe_2O_4$ and CuFeO exhibited the high catalytic properties for SMX and SMZ at neutral pH condition, respectively [184,185]. Compared with 3D mesoporous $CuFe_2O_4$, CuFeO presented a better chemical stability. After 30 min reaction, the leaching amount of Cu and Fe was only 2.10 mg L^{-1} and 1.31 mg L^{-1}, respectively (Fig. 14a). And the removal percentage of SMZ was nearly 100% in ultrapure water, tap water and river water (Fig. 14b). As shown in Fig. 14c, •OH radicals and photo-induced e^- were the main reactive species. Copper and iron species in the catalyst structure were effectively excited by visible light and transfer e^- to H_2O_2, generating •OH radicals. And then the formed •OH reacted with SMZ to form the final degradation products [184]. The results indicated that copper-iron oxide is a promising catalyst for SNs degradation.

Nowadays, electro-Fenton has been widely used in SNs removal due to its remarkable advantages such as H_2O_2 can be generated in situ by oxygen reduction reaction (ORR) (Eq. (3)), the generation of Fe^{2+} on the cathode (Eq. (4)) and reduction of accumulation of waste iron sludge [186]. According to the literature [183], the boron doped

Table 4
The applications of various Fenton process in removing SNs.

Iron source	SNs	Experimental conditions	Removal efficiency	Remarks	Ref.
$FeSO_4$ (179 μM)	SMX	$[SMX]_0$ = 158 μM, H_2O_2 = 100 μM, reaction time = 50 min, pH = 3.	99.7%	The Fenton system had a strong dependence on Fe^{2+} concentration.	[177]
$FeCl_3$ (360 μM)		$[SMX]_0$ = 158 μM, H_2O_2 = 100 μM, reaction time = 50 min, pH = 3.	91.5%	The Fenton-like system had a strong dependence on Fe^{3+} concentration.	[177]
3D mesoporous $CuFe_2O_4$ (0.2 g L^{-1})		$[SMX]_0$ = 10 mg L^{-1}, H_2O_2 = 10 mM, pH = 6.73, reaction time = 2 h, under simulated sunlight.	96%	3D mesoporous $CuFe_2O_4$ exhibited good circularity.	[185]
$FeSO_4$ (0.2 mM)	SFZ	$[SFZ]_0$ = 20 mg L^{-1}, H_2O_2 = 10 mM, pH = 3, reaction time = 60 min, under UV condition.	90%	The photo-Fenton system had slightly dependence on Fe^{2+} concentration.	[190]
$Fe_2(SO_4)_3$ (0.2 mM)		$[SFZ]_0$ = 20 mg L^{-1}, H_2O_2 = 10 mM, pH = 3, reaction time = 60 min, under UV condition.	88%	The photo-Fenton like system had slightly dependence on Fe^{3+} concentration.	[190]
Pyrite (2.0 g L^{-1})	SMZ	$[SMZ]_0$ = 0.2 mM, reaction time = 80 min, pH = 3, current intensity = 1000 mA.	95%	Pyrite-EF showed a better mineralization performance compared with EF.	[183]
Co-SAM-SCS (0.7 g L^{-1})		$[SMZ]_0$ = 50 mg L^{-1}, H_2O_2 = 2%, reaction time = 240 min, pH = 7, under visible light.	96.72%	Co-SAM-SCS exhibited good stability.	[191]
CuFeO (500 mg L^{-1})		$[SMZ]_0$ = 500 mg L^{-1}, H_2O_2 = 60 mM, reaction time = 30 min, pH = 6, under visible light.	95.42%	Both Cu and Fe in CuFeO presented good performance.	[184]
Fe_3O_4-Mn_3O_4/rGO (0.5 g L^{-1})		$[SMZ]_0$ = 0.07 mM, H_2O_2 = 6 mM, reaction time = 2 h, pH = 3, T = 35 °C.	98%	The catalyst exhibited good stability. The removal percentage still remained 82% after five cycles.	[192]

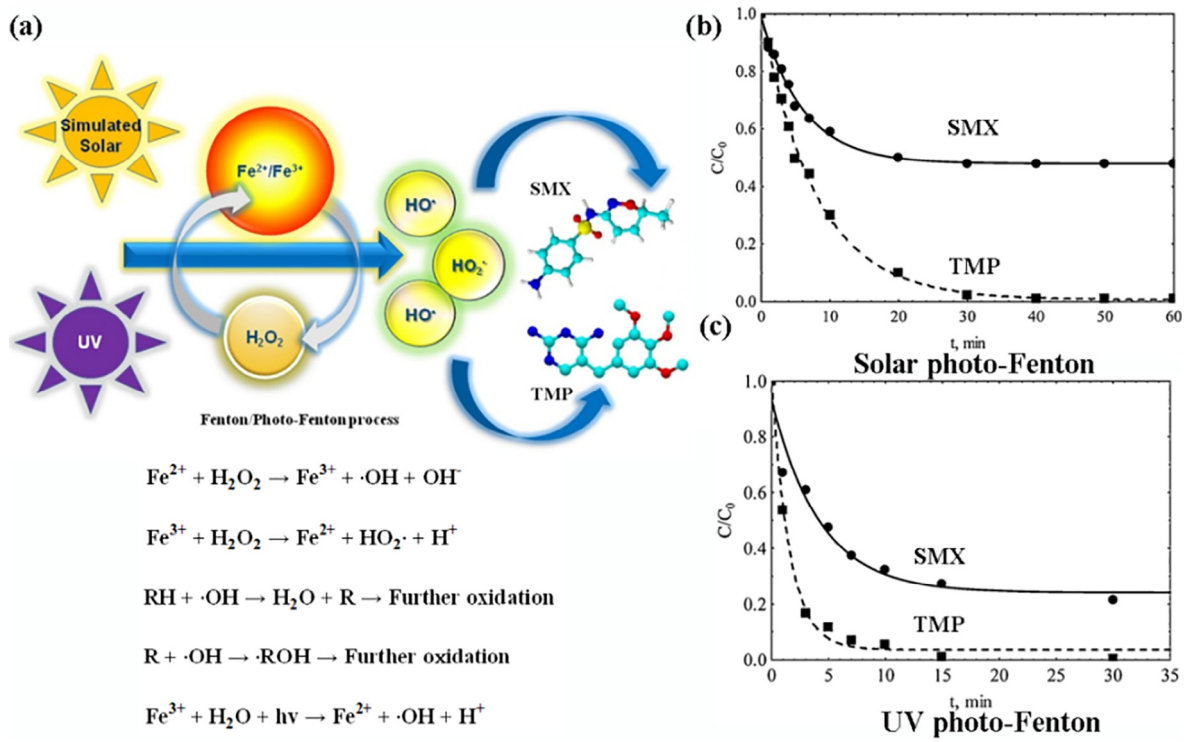

Fig. 13. (a) The degradation mechanism of SMX and TMP by Fenton/photo-Fenton process. Simultaneous degradation of SMX and TMP in solar photo-Fenton (b) and solar photo-Fenton (c). Reproduced with permission from Ref. [177]. Copyright 2018, Elsevier.

diamond (BDD) anode was better than Pt anode when carbon-felt as cathode in removal percentage (95% vs 87%) and mineralization rate (90% vs 83%). This is because BDD anode can produce more O_2 (oxidation of H_2O molecules), increasing the dissolved O_2 to form more H_2O_2, thus promoting the formation of •OH. Besides, when the cathode was carbon nitride modified gas diffusion electrode (g-C3N4@GDE) and the anode was BDD [187], the electro-Fenton system presented a high catalytic performance (Reaction condition: $[STZ]_0 = 500\ mg\ L^{-1}$, $[Fe^{2+}] = 100\ \mu M$, current = 50 Ma and pH = 3): 457.45 μM of H_2O_2 was produced and the removal percentage of STZ was nearly 100% after 180 min electrolysis [187]. Deng et al. [188] prepared B@Ni-F cathode with waste giant reed, and the fabrication process is depicted in Fig. 15. The first step was to carbonize the washed giant reed for 6 h at 260 °C in air. Then, the carbonized giant reed was transferred to quartz tube furnace for complete pyrolysis in N_2 at 500 °C for 2 h. Finally, the prepared N-doped BC was immobilized on Ni-F by rolling approach [188]. Results showed that the amount of H_2O_2 accumulation on B@Ni-F cathode was enhanced 14 times compared to original Ni-F cathode, which was mainly attributed to the abundant oxygen and nitrogen functional groups on BC surface, and it improved the hydrophilicity of the cathode (Fig. 15). Besides, the presence of pyridine N facilitated H_2O_2 generation because carbon atom adjacent to pyridine N was the active site of ORR [189].

$$O_2 + 2H^+ + 2e^- \rightarrow H_2O_2 \quad (3)$$

$$Fe^{3+} + e^- \rightarrow Fe^{2+} \quad (4)$$

6. Evaluation of the intermediates toxicity and degradation pathway

Considering the fact that SNs degradation intermediates have been identified as potential toxicity or even higher toxicity [193,194], it is necessary to evaluate the degradation pathway and its intermediates toxicity. According to the literature [177], approximately 100% SMX removal efficiency was achieved in UV, UV/H_2O_2, Solar/Fe^{3+}/H_2O_2 systems, but the solution toxicity significantly increased in UV/H_2O_2 system. By contrast, SMX solutions treated by solar alone were relatively less toxic. Barhoumi et al. [183] selected *Vibrio fischeri* to evaluate the toxicity evolution of SMZ solution in electron-Fenton. Results showed that the aromatic compounds in the early stages of electrolysis (15 min) have a high toxicity level. Subsequently, these compounds were attacked by •OH, causing a high mineralization, thereby reducing the toxicity of the solution [183].

Furthermore, Deng et al. [188] investigated SMR degradation pathways and its intermediates toxicity in detail. As shown in Fig. 16a, the hydroxylation of aniline residues in SMR was the dominant degradation pathway, leading to the formation of $C_{11}H_{12}N_4O_3S$. Subsequently, the cleavage of S-N bond was occurred. This is because several average local ionization energy (ALIE) minima points existed around the S-N bond, including 9.15, 8.94, 9.22 and 9.29 eV (Fig. 16b). These sites were prone to electrophilic and free radical reactions. Then the aromatic rings of these compounds were destroyed to form various small molecules such as carboxylic acids, CO_2 and H_2O [188]. The degradation pathway mentioned above was in good agreement with the degradation pathway of SMX in WO_3-g-C_3N_4 photocatalyst system [157]. And the toxicity evolution of SMR ($50\ mg\ L^{-1}$) after 6 h electrolysis was displayed in Fig. 16c. The original SMR solutions exhibited 30.82% bioluminescence inhibition. After 60 min electrolysis, the inhibition rised to 89%, suggesting that high toxicity intermediates were generated, such as *p*-benzoquinone (BQ). Subsequently, the inhibition was significantly reduced, eventually reaching 20%. The toxicity trend was in accordance with Barhoumi's investigations [183].

From the above results, incomplete mineralization of SNs may lead to the increase of acute toxicity. Therefore, there should be more consideration on the treatment residual in the practical cases to avoid the occurrence of unnatural toxic events. It also shows that electro-Fenton system may be an effective approach for SNs detoxification. Hydroxylation, and the cleavage of S-N bond were regarded as the dominant degradation pathways during SNs oxidation when •OH and $SO_4^{\bullet -}$ were involved.

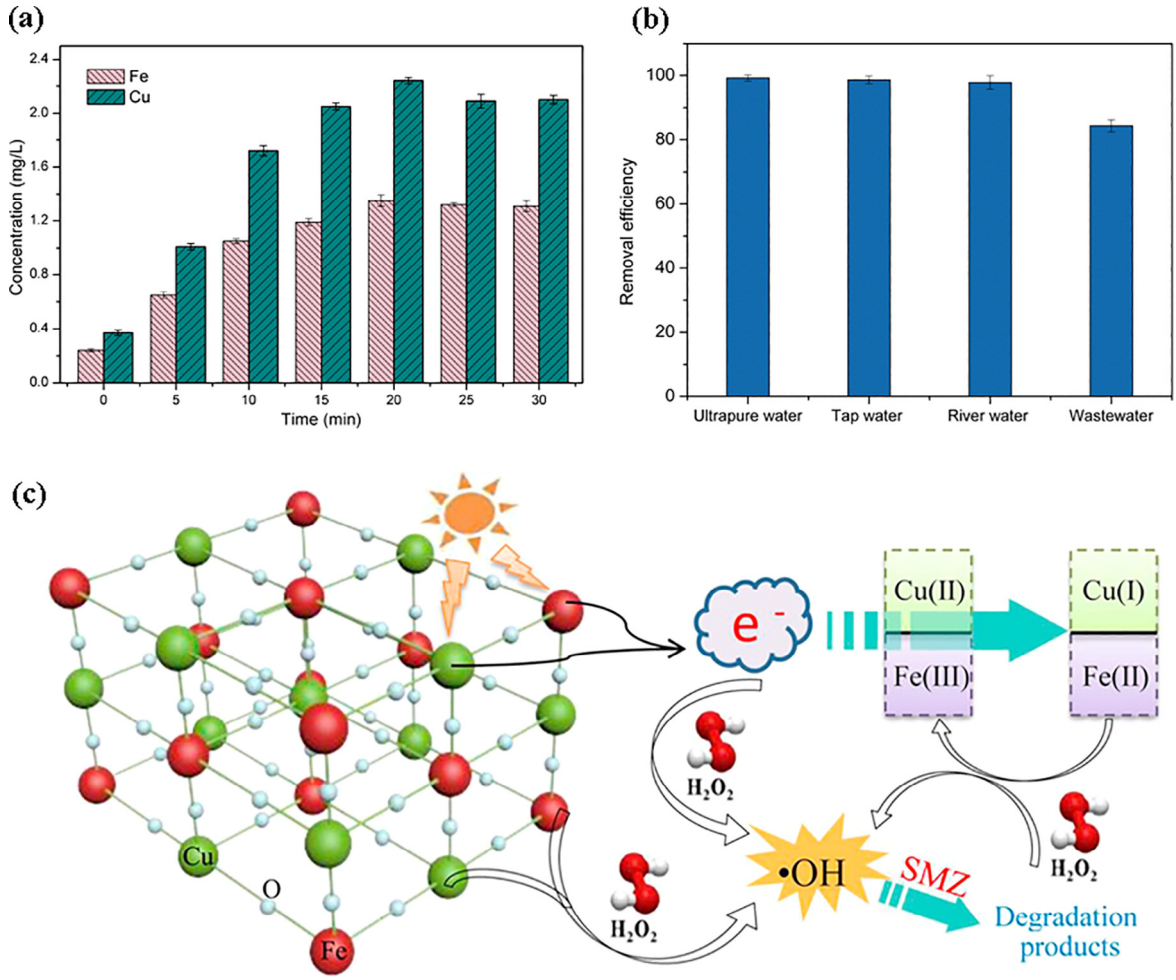

Fig. 14. (a) The chemical stability of CuFeO. (b) Removal percentage of SMZ in different wastewater (Reaction conditions: $[SMZ]_0$ = 50 mg/L; $[CuFeO]_0$ = 500 mg/L; pH = 6; T = 20 °C). (c) Degradation mechanism of SMZ in CuFeO photo-Fenton system. Reproduced with permission from Ref. [184]. Copyright 2019, Elsevier.

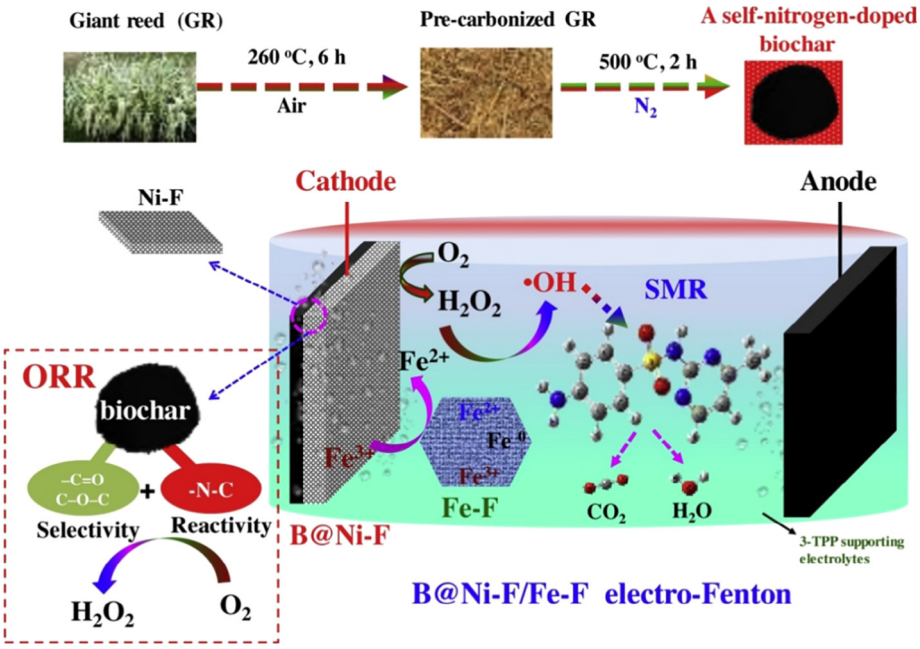

Fig. 15. Schematic illustration for the fabrication process of B@Ni-F cathode and mechanism for B@Ni-F/Fe-F in electro-Fenton system. Reproduced with permission from Ref. [188]. Copyright 2019, Elsevier.

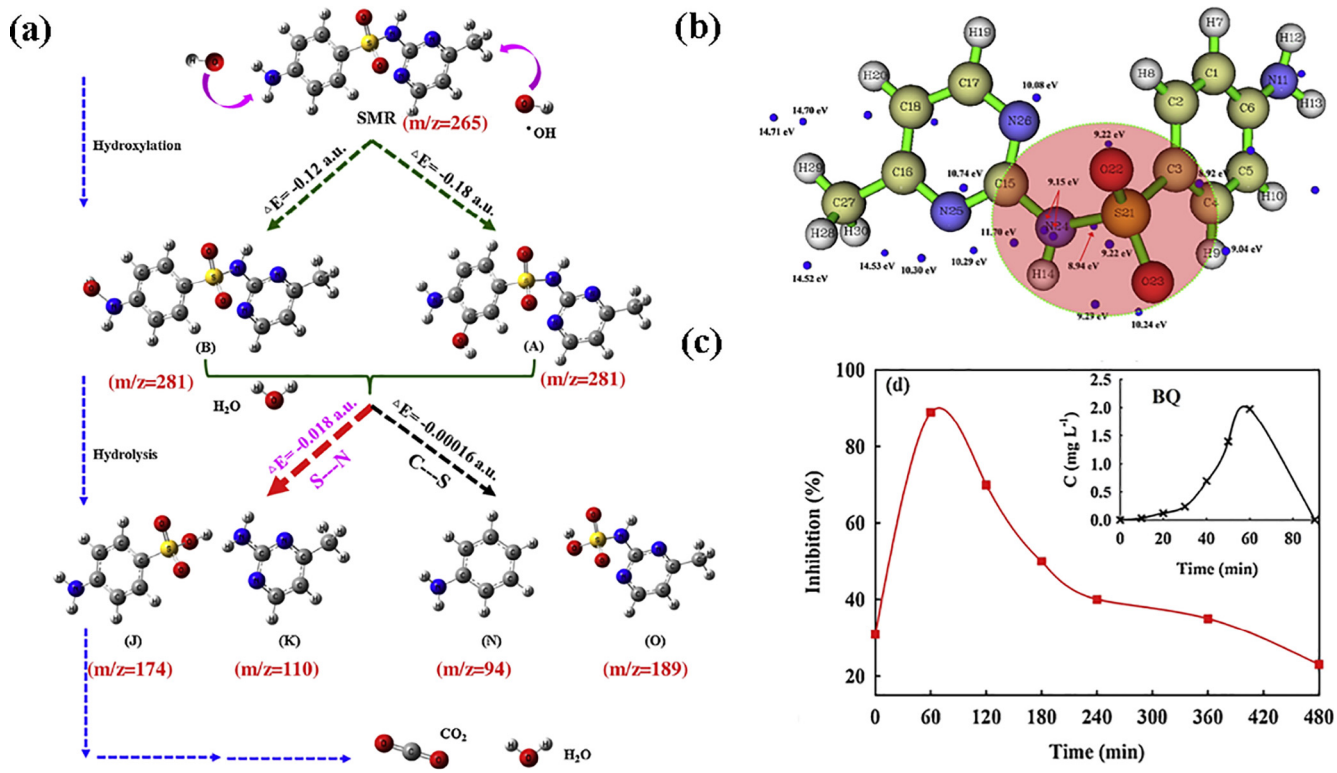

Fig. 16. (a) SMR degradation pathway in B@Ni-F/Fe-F electro-Fenton system. (b) Average local ionization energy analysis for SMR. (c) Evolution of solution toxicity. Reproduced with permission from Ref. [188]. Copyright 2019, Elsevier.

7. Conclusions and future challenges

This review provides important information on SNs occurrence, fate, distribution, removal techniques and toxicity assessment. Adsorption and AOPs are mainstream technologies for the removal of SNs. As a whole, the integration of adsorbent materials into AOPs will be the future development trend. The integrated technique could effectively increase the removal efficiency through the synergistic effect, and possess the advantages of both AOPs and adsorption. However, whether single or multiple processes, the removal efficiency of SNs is very susceptible to various parameters such as solution pH and matrix components. In the process of adsorption, potential adsorption mechanisms include EDA interaction, CAHB interaction, Lewis acid-base interaction, electrostatic interaction, hydrophobic interaction, H-bonding, pore-filling and Van der Waals forces. EDA interaction, CAHB interaction and hydrophobic interaction are widely regarded as the primary adsorption mechanism. In AOPs system, h^+, •OH, $SO_4^{\bullet-}$ and $O_2^{\bullet-}$ are highly reactive species. The degradation pathways of SNs mainly include hydroxylation of the benzene ring, cleavage of N-S bond, heterocyclic smile-rearrangement, carboxylation of the methyl group, and nitration and nitrosation of amino group. In general, hydroxylation and cleavage of N-S bond are their common degradation pathways. However, it is worth noting that there are still many issues to be addressed.

Firstly, SNs contain two types of heterocycle rings (*hexa*-heterocycle and penta-heterocycle). Five- and six-membered SNs possess different electron densities, thus existing different degradation pathways and removal efficiency. Therefore, the adsorption affinities and degradation pathways of the two types of SNs are needed to be further investigated, which allows for comprehending their adsorption and degradation mechanisms. In addition, more toxicity assessment studies should be performed to determine whether the by-products can meet environmental requirements because some intermediates may be more acute toxicity than their original compounds.

Secondly, most experiments are at the laboratory level, but the concentration of SNs in the actual wastewater (ng L^{-1}–μg L^{-1}) is much lower than that of the experimental model wastewater (mg L^{-1}), and the composition is extremely complex in natural environment. There may be competitive effects and shielding effects, eventually leading to lower adsorption capacity and slower reactivity. Thus, it is necessary to investigate the removal mechanisms and behaviors of SNs within different natural environment systems.

Thirdly, most of studies were remained in aqueous solution. There are few studies in soils and sediments environment. However, the persistent nature of SNs resistance genes in soils is high, even at low concentration levels. The resistance genes could enter human body through food chain, further impacting human health. Sediments act as the sink and source of water pollution. When water environment conditions change such as floods and acidification, SNs immobilized in sediments may be recycled back to the aqueous phase, causing secondary pollution. Therefore, further investigations are required to evaluate the application of these techniques in soils and sediments.

Fourthly, the release of contaminants from various adsorbents occurs frequently, leading to the limitation of their application. Meanwhile, dissolved organic carbons possess photochemical activity, while their availabilities and ecological risks are still uncertain. Thus, the stability and activity of carbon materials will be the focus of future researches.

Acknowledgements

This study was financially supported by the Program for the National Natural Science Foundation of China (51809090, 51879101, 51579098, 51779090, 51709101, 51521006, 51278176, 51378190), the National Program for Support of Top–Notch Young Professionals of China (2014), the Program for Changjiang Scholars and Innovative Research Team in University (IRT-13R17), and Hunan Provincial Science and Technology Plan Project (2018SK20410, 2017SK2243,

2016RS3026), the Natural Science Foundation of Hunan Province, China (Grant Nos. 2019JJ50077), and the Fundamental Research Funds for the Central Universities (531118010114, 531119200086, 531107050978).

References

[1] I.T. Carvalho, L. Santos, Antibiotics in the aquatic environments: a review of the European scenario, Environ. Int. 94 (2016) 736–757.
[2] J. Hou, W. Wan, D. Mao, C. Wang, Q. Mu, S. Qin, Y. Luo, Occurrence and distribution of sulfonamides, tetracyclines, quinolones, macrolides, and nitrofurans in livestock manure and amended soils of Northern China, Environ. Sci. Pollut. Res. 22 (2014) 4545–4554.
[3] M. Conde-Cid, C. Álvarez-Esmorís, R. Paradelo-Núñez, J.C. Nóvoa-Muñoz, M. Arias-Estévez, E. Álvarez-Rodríguez, M.J. Fernández-Sanjurjo, A. Núñez-Delgado, Occurrence of tetracyclines and sulfonamides in manures, agricultural soils and crops from different areas in Galicia (NW Spain), J. Clean. Prod. 197 (2018) 491–500.
[4] E.Y. Klein, T.P. Van Boeckel, E.M. Martinez, S. Pant, S. Gandra, S.A. Levin, H. Goossens, R. Laxminarayan, Global increase and geographic convergence in antibiotic consumption between 2000 and 2015, Proc. Natl. Acad. Sci. U.S.A. 115 (2018) E3463–E3470.
[5] Q.Q. Zhang, G.G. Ying, C.G. Pan, Y.S. Liu, J.L. Zhao, Comprehensive evaluation of antibiotics emission and fate in the river basins of China: source analysis, multimedia modeling, and linkage to bacterial resistance, Environ. Sci. Technol. 49 (2015) 6772–6782.
[6] W. Baran, E. Adamek, J. Ziemiańska, A. Sobczak, Effects of the presence of sulfonamides in the environment and their influence on human health, J. Hazard. Mater. 196 (2011) 1–15.
[7] Y.L. Lye, C.W. Bong, C.W. Lee, R.J. Zhang, G. Zhang, S. Suzuki, L.C. Chai, Anthropogenic impacts on sulfonamide residues and sulfonamide resistant bacteria and genes in Larut and Sangga Besar River, Perak, Sci. Total Environ. 688 (2019) 1335–1347.
[8] M. Conde-Cid, D. Fernandez-Calvino, J.C. Novoa-Munoz, M. Arias-Estevez, M. Diaz-Ravina, A. Nunez-Delgado, M.J. Fernandez-Sanjurjo, E. Alvarez-Rodriguez, Degradation of sulfadiazine, sulfachloropyridazine and sulfamethazine in aqueous media, J. Environ. Manage. 228 (2018) 239–248.
[9] C. Li, J. Chen, J. Wang, Z. Ma, P. Han, Y. Luan, A. Lu, Occurrence of antibiotics in soils and manures from greenhouse vegetable production bases of Beijing, China and an associated risk assessment, Sci. Total Environ. 521–522 (2015) 101–107.
[10] C. Zhang, J. Tang, L. Wang, X. Gao, X. He, Occurrence of Antibiotics in Water and Sediment from Zizhuyuan Lake, Pol. J. Environ. Studies 24 (2015) 1831–1836.
[11] X. Liu, S. Lu, W. Guo, B. Xi, W. Wang, Antibiotics in the aquatic environments: a review of lakes, China, Sci. Total Environ. 627 (2018) 1195–1208.
[12] S. Li, W. Shi, W. Liu, H. Li, W. Zhang, J. Hu, Y. Ke, W. Sun, J. Ni, A duodecennial national synthesis of antibiotics in China's major rivers and seas (2005–2016), Sci. Total Environ. 615 (2018) 906–917.
[13] A. Christou, A. Aguera, J.M. Bayona, E. Cytryn, V. Fotopoulos, D. Lambropoulou, C.M. Manaia, C. Michael, M. Revitt, P. Schroder, D. Fatta-Kassinos, The potential implications of reclaimed wastewater reuse for irrigation on the agricultural environment: The knowns and unknowns of the fate of antibiotics and antibiotic resistant bacteria and resistance genes – A review, Water Res. 123 (2017) 448–467.
[14] M.B. Ahmed, J.L. Zhou, H.H. Ngo, W. Guo, N.S. Thomaidis, J. Xu, Progress in the biological and chemical treatment technologies for emerging contaminant removal from wastewater: A critical review, J. Hazard. Mater. 323 (2017) 274–298.
[15] X.Y. Guo, Z.W. Peng, D.L. Huang, P. Xu, G.M. Zeng, S. Zhou, X.M. Gong, M. Cheng, R. Deng, H. Yi, H. Luo, X.L. Yan, T. Li, Biotransformation of cadmium-sulfamethazine combined pollutant in aqueous environments: Phanerochaete chrysosporium bring cautious optimism, Chem. Eng. J. 347 (2018) 74–83.
[16] K.L. Chen, L.C. Liu, W.R. Chen, Adsorption of sulfamethoxazole and sulfapyridine antibiotics in high organic content soils, Environ. Pollut. 231 (2017) 1163–1171.
[17] C. Lai, M. Zhang, B. Li, D. Huang, G. Zeng, L. Qin, X. Liu, H. Yi, M. Cheng, L. Li, Z. Chen, L. Chen, Fabrication of CuS/$BiVO_4$ (040) binary heterojunction photocatalysts with enhanced photocatalytic activity for Ciprofloxacin degradation and mechanism insight, Chem. Eng. J. 358 (2019) 891–902.
[18] Y. Yang, Z. Zeng, C. Zhang, D. Huang, G. Zeng, R. Xiao, C. Lai, C. Zhou, H. Guo, W. Xue, M. Cheng, W. Wang, J. Wang, Construction of iodine vacancy-rich BiOI/Ag@AgI Z-scheme heterojunction photocatalysts for visible-light-driven tetracycline degradation: transformation pathways and mechanism insight, Chem. Eng. J. 349 (2018) 808–821.
[19] D. Kanakaraju, B.D. Glass, M. Oelgemoller, Advanced oxidation process-mediated removal of pharmaceuticals from water: a review, J. Environ. Manage. 219 (2018) 189–207.
[20] D. Jiang, P. Xu, H. Wang, G. Zeng, D. Huang, M. Chen, C. Lai, C. Zhang, J. Wan, W. Xue, Strategies to improve metal organic frameworks photocatalyst's performance for degradation of organic pollutants, Coord. Chem. Rev. 376 (2018) 449–466.
[21] C. Zhang, W. Wang, A. Duan, G. Zeng, D. Huang, C. Lai, X. Tan, M. Cheng, R. Wang, C. Zhou, W. Xiong, Y. Yang, Adsorption behavior of engineered carbons and carbon nanomaterials for metal endocrine disruptors: Experiments and theoretical calculation, Chemosphere 222 (2019) 184–194.
[22] M. Xie, W. Chen, Z. Xu, S. Zheng, D. Zhu, Adsorption of sulfonamides to demineralized pine wood biochars prepared under different thermochemical conditions, Environ. Pollut. 186 (2014) 187–194.
[23] Q.Q. Yang, G.C. Chen, J.F. Zhang, H.L. Li, Adsorption of sulfamethazine by multi-walled carbon nanotubes: effects of aqueous solution chemistry, RSC Adv. 5 (2015) 25541–25549.
[24] C. Lai, M.M. Wang, G.M. Zeng, Y.G. Liu, D.L. Huang, C. Zhang, R.Z. Wang, P. Xu, M. Cheng, C. Huang, H.P. Wu, L. Qin, Synthesis of surface molecular imprinted TiO_2/graphene photocatalyst and its highly efficient photocatalytic degradation of target pollutant under visible light irradiation, Appl. Surf. Sci. 390 (2016) 368–376.
[25] M. Cheng, C. Lai, Y. Liu, G.M. Zeng, D.L. Huang, C. Zhang, L. Qin, L. Hu, C.Y. Zhou, W.P. Xiong, Metal-organic frameworks for highly efficient heterogeneous Fenton-like catalysis, Coord. Chem. Rev. 368 (2018) 80–92.
[26] S. Babić, A.J.M. Horvat, D. Mutavdžić Pavlović, M. Kaštelan-Macan, Determination of pKa values of active pharmaceutical ingredients, TrAC Trends in Anal.l, Chem. 26 (2007) 1043–1061.
[27] C. Peiris, S.R. Gunatilake, T.E. Mlsna, D. Mohan, M. Vithanage, Biochar based removal of antibiotic sulfonamides and tetracyclines in aquatic environments: a critical review, Bioresour. Technol. 246 (2017) 150–159.
[28] F. Yu, Y. Li, S. Han, J. Ma, Adsorptive removal of antibiotics from aqueous solution using carbon materials, Chemosphere 153 (2016) 365–385.
[29] J.T. Wu, C.H. Wu, C.Y. Liu, W.J. Huang, Photodegradation of sulfonamide antimicrobial compounds (sulfadiazine, sulfamethizole, sulfamethoxazole and sulfathiazole) in various UV/oxidant systems, Water Sci. Technol. 71 (2015) 412–417.
[30] J. Lian, Z. Qiang, M. Li, J.R. Bolton, J. Qu, UV photolysis kinetics of sulfonamides in aqueous solution based on optimized fluence quantification, Water Res. 75 (2015) 43–50.
[31] M.B. Ahmed, J.L. Zhou, H.H. Ngo, W. Guo, Adsorptive removal of antibiotics from water and wastewater: progress and challenges, Sci. Total Environ. 532 (2015) 112–126.
[32] X.Q. Yu, L.P. Zhang, M. Liang, W.L. Sun, pH-dependent sulfonamides adsorption by carbon nanotubes with different surface oxygen contents, Chem. Eng. J. 279 (2015) 363–371.
[33] M.B. Ahmed, J.L. Zhou, H.H. Ngo, W. Guo, M.A.H. Johir, K. Sornalingam, Single and competitive sorption properties and mechanism of functionalized biochar for removing sulfonamide antibiotics from water, Chem. Eng. J. 311 (2017) 348–358.
[34] C. Zhou, C. Lai, D. Huang, G. Zeng, C. Zhang, M. Cheng, L. Hu, J. Wan, W. Xiong, M. Wen, X. Wen, L. Qin, Highly porous carbon nitride by supramolecular preassembly of monomers for photocatalytic removal of sulfamethazine under visible light driven, Appl. Catal., B 220 (2018) 202–210.
[35] B.J. Dang, D.Q. Mao, Y. Xu, Y. Luo, Conjugative multi-resistant plasmids in Haihe River and their impacts on the abundance and spatial distribution of antibiotic resistance genes, Water Res. 111 (2017) 81–91.
[36] R. Hirsch, T. Ternes, K. Haberer, K.L. Kratz, Occurrence of antibiotics in the aquatic environment, Sci. Total Environ. 225 (1999) 109–118.
[37] K.J.C. Kā¼Mmerer, Antibiotics in the aquatic environment–a review–part I, Chemosphere 75 (2009) 417–434.
[38] K.J.C. Kā¼Mmerer, Antibiotics in the aquatic environment–a review–part II, Chemosphere 75 (2009) 435–441.
[39] Y. Valcarcel, S.G. Alonso, J.L. Rodriguez-Gil, A. Gil, M. Catala, Detection of pharmaceutically active compounds in the rivers and tap water of the Madrid Region (Spain) and potential ecotoxicological risk, Chemosphere 84 (2011) 1336–1348.
[40] B. Subedi, N. Codru, D.M. Dziewulski, L.R. Wilson, J. Xue, S. Yun, E. Braun-Howland, C. Minihane, K. Kannan, A pilot study on the assessment of trace organic contaminants including pharmaceuticals and personal care products from on-site wastewater treatment systems along Skaneateles Lake in New York State, USA, Water Res. 72 (2015) 28–39.
[41] Y. Luo, L. Xu, M. Rysz, Y. Wang, H. Zhang, P.J. Alvarez, Occurrence and transport of tetracycline, sulfonamide, quinolone, and macrolide antibiotics in the Haihe River Basin, China, Environ. Sci. Technol. 45 (2011) 1827–1833.
[42] Y. Xu, C. Guo, J. Lv, S. Hou, Y. Luo, Y. Zhang, J. Xu, Spatiotemporal profile of tetracycline and sulfonamide and their resistance on a catchment scale, Environ. Pollut. 241 (2018) 1098–1105.
[43] C. Wu, X. Huang, J.D. Witter, A.L. Spongberg, K. Wang, D. Wang, J. Liu, Occurrence of pharmaceuticals and personal care products and associated environmental risks in the central and lower Yangtze river, China, Ecotoxicol. Environ. Saf. 106 (2014) 19–26.
[44] C. Wu, A.L. Spongberg, J.D. Witter, Use of solid phase extraction and liquid chromatography-tandem mass spectrometry for simultaneous determination of various pharmaceuticals in surface water, Int. J. Environ. Anal. Chem. 88 (2008) 1033–1048.
[45] P.J. Ferguson, M.J. Bernot, J.C. Doll, T.E. Lauer, Detection of pharmaceuticals and personal care products (PPCPs) in near-shore habitats of southern Lake Michigan, Sci. Total Environ. 458–460 (2013) 187–196.
[46] C. Nguyen Dang Giang, Z. Sebesvari, F. Renaud, I. Rosendahl, Q. Hoang Minh, W. Amelung, Occurrence and Dissipation of the Antibiotics Sulfamethoxazole, Sulfadiazine, Trimethoprim, and Enrofloxacin in the Mekong Delta, Vietnam, PLoS One 10 (2015) e0131855.
[47] G.G.M. Jesús, D.C.M. Silvia, B. Damià, Occurrence of sulfonamide residues along the Ebro River basin: removal in wastewater treatment plants and environmental impact assessment, Environ. Pollut. 37 (2011) 462–473.
[48] W. Baran, E. Adamek, J. Ziemianska, A. Sobczak, Effects of the presence of sulfonamides in the environment and their influence on human health, J. Hazard. Mater. 196 (2011) 1–15.
[49] S. Jechalke, H. Heuer, J. Siemens, W. Amelung, K. Smalla, Fate and effects of

veterinary antibiotics in soil, Trends Microbiol. 22 (2014) 536–545.
[50] N. Wang, X. Guo, J. Xu, L. Hao, D. Kong, S. Gao, Sorption and transport of five sulfonamide antibiotics in agricultural soil and soil-manure systems, J. Environ. Sci. Health., Part B 50 (2015) 23–33.
[51] U. Hammesfahr, A. Kotzerke, M. Lamshöft, B.-M. Wilke, E. Kandeler, S. Thiele-Bruhn, Effects of sulfadiazine-contaminated fresh and stored manure on a soil microbial community, Eur. J. Soil Biol. 47 (2011) 61–68.
[52] A. Kotzerke, S. Sharma, K. Schauss, H. Heuer, S. Thiele-Bruhn, K. Smalla, B.M. Wilke, M. Schloter, Alterations in soil microbial activity and N-transformation processes due to sulfadiazine loads in pig-manure, Environ. pollut. 153 (2008) 315–322.
[53] R. Reichel, I. Rosendahl, E.T.H.M. Peeters, A. Focks, J. Groeneweg, R. Bierl, A. Schlichting, W. Amelung, S. Thiele-Bruhn, Effects of slurry from sulfadiazine-(SDZ) and difloxacin- (DIF) medicated pigs on the structural diversity of microorganisms in bulk and rhizosphere soil, Soil Biol. Biochem. 62 (2013) 82–91.
[54] P. Grenni, V. Ancona, A. Barra Caracciolo, Ecological effects of antibiotics on natural ecosystems: a review, Microchem. J. 136 (2018) 25–39.
[55] H. Yang, S. Zhuang, Q. Hu, L. Hu, L. Yang, C. Au, B. Yi, Competitive reactions of hydroxyl and sulfate radicals with sulfonamides in $Fe^{2+}/S_2O_8^{2-}$ system: Reaction kinetics, degradation mechanism and acute toxicity, Chem. Eng. J. 339 (2018) 32–41.
[56] M. Pan, L.M. Chu, Phytotoxicity of veterinary antibiotics to seed germination and root elongation of crops, Ecotoxicol Environ Saf 126 (2016) 228–237.
[57] M. Pan, L.M. Chu, Fate of antibiotics in soil and their uptake by edible crops, The Sci. Total Environ. 599–600 (2017) 500–512.
[58] A. Bialk-Bielinska, M. Caban, A. Pieczynska, P. Stepnowski, S. Stolte, Mixture toxicity of six sulfonamides and their two transformation products to green algae Scenedesmus vacuolatus and duckweed Lemna minor, Chemosphere 173 (2017) 542–550.
[59] J.J. Pignatello, W.A. Mitch, W. Xu, Activity and reactivity of pyrogenic carbonaceous matter toward organic compounds, Environ. Sci. Technol. 51 (2017) 8893–8908.
[60] F. Xiao, J.J. Pignatello, pi(+)-pi interactions between (hetero)aromatic amine cations and the graphitic surfaces of pyrogenic carbonaceous materials, Environ. Sci. Technol. 49 (2015) 906–914.
[61] M. Kah, G. Sigmund, F. Xiao, T. Hofmann, Sorption of ionizable and ionic organic compounds to biochar, activated carbon and other carbonaceous materials, Water Res. 124 (2017) 673–692.
[62] A.U. Rajapaksha, M. Vithanage, M. Zhang, M. Ahmad, D. Mohan, S.X. Chang, Y.S. Ok, Pyrolysis condition affected sulfamethazine sorption by tea waste biochars, Bioresour. Technol. 166 (2014) 303–308.
[63] Y.K. Choi, E. Kan, Effects of pyrolysis temperature on the physicochemical properties of alfalfa-derived biochar for the adsorption of bisphenol A and sulfamethoxazole in water, Chemosphere 218 (2018) 741–748.
[64] M.B. Ahmed, J.L. Zhou, H.H. Ngo, W. Guo, M.A.H. Johir, D. Belhaj, Competitive sorption affinity of sulfonamides and chloramphenicol antibiotics toward functionalized biochar for water and wastewater treatment, Bioresour. Technol. 238 (2017) 306–312.
[65] J. Luo, X. Li, C. Ge, K. Muller, H. Yu, P. Huang, J. Li, D.C.W. Tsang, N.S. Bolan, J. Rinklebe, H. Wang, Sorption of norfloxacin, sulfamerazine and oxytetracycline by KOH-modified biochar under single and ternary systems, Bioresour. Technol. 263 (2018) 385–392.
[66] A.U. Rajapaksha, M. Vithanage, M. Ahmad, D.C. Seo, J.S. Cho, S.E. Lee, S.S. Lee, Y.S. Ok, Enhanced sulfamethazine removal by steam-activated invasive plant-derived biochar, J. Hazard. Mater. 290 (2015) 43–50.
[67] C.B. Vidal, M. Seredych, E. Rodriguez-Castellon, R.F. Nascimento, T.J. Bandosz, Effect of nanoporous carbon surface chemistry on the removal of endocrine disruptors from water phase, J. Colloid Interface Sci. 449 (2015) 180–191.
[68] J. Wan, H. Deng, J. Shi, L. Zhou, T. Su, Synthesized magnetic manganese ferrite nanoparticles on activated carbon for sulfamethoxazole removal, CLEAN-Soil. Air. Water. 42 (2014) 1199–1207.
[69] Y. Liu, X. Liu, W. Dong, L. Zhang, Q. Kong, W. Wang, Efficient adsorption of sulfamethazine onto modified activated carbon: a plausible adsorption mechanism, Sci. Rep. 7 (2017) 12437.
[70] F.F. Liu, J. Zhao, S. Wang, B. Xing, Adsorption of sulfonamides on reduced graphene oxides as affected by pH and dissolved organic matter, Environ. Pollut. 210 (2016) 85–93.
[71] H. Chen, B. Gao, H. Li, Functionalization, pH, and ionic strength influenced sorption of sulfamethoxazole on graphene, J. Environ. Chem. Eng. 2 (2014) 310–315.
[72] S.W. Nam, C. Jung, H. Li, M. Yu, J.R. Flora, L.K. Boateng, N. Her, K.D. Zoh, Y. Yoon, Adsorption characteristics of diclofenac and sulfamethoxazole to graphene oxide in aqueous solution, Chemosphere 136 (2015) 20–26.
[73] B. Peng, L. Chen, C. Que, K. Yang, F. Deng, X. Deng, G. Shi, G. Xu, M. Wu, Adsorption of antibiotics on graphene and biochar in aqueous solutions induced by pi-pi Interactions, Sci. Rep. 6 (2016) 31920.
[74] F. Wang, W. Sun, W. Pan, N. Xu, Adsorption of sulfamethoxazole and 17β-estradiol by carbon nanotubes/$CoFe_2O_4$ composites, Chem. Eng. J. 274 (2015) 17–29.
[75] M. Inyang, B. Gao, A. Zimmerman, Y. Zhou, X. Cao, Sorption and cosorption of lead and sulfapyridine on carbon nanotube-modified biochars, Environ. Sci. Pollut. 22 (2015) 1868–1876.
[76] M.R. Azhar, H.R. Abid, H. Sun, V. Periasamy, M.O. Tade, S. Wang, Excellent performance of copper based metal organic framework in adsorptive removal of toxic sulfonamide antibiotics from wastewater, J. Colloid Interface Sci. 478 (2016) 344–352.
[77] X. Huang, Q. Hu, L. Gao, Q. Hao, P. Wang, D. Qin, Adsorption characteristics of metal–organic framework MIL-101(Cr) towards sulfamethoxazole and its persulfate oxidation regeneration, RSC Adv. 8 (2018) 27623–27630.
[78] Y. Gao, R. Kang, J. Xia, G. Yu, S. Deng, Understanding the adsorption of sulfonamide antibiotics on MIL-53s: Metal dependence of breathing effect and adsorptive performance in aqueous solution, J. Colloid Interface Sci. 535 (2019) 159–168.
[79] M.R. Azhar, H.R. Abid, V. Periasamy, H. Sun, M.O. Tade, S. Wang, Adsorptive removal of antibiotic sulfonamide by UiO-66 and ZIF-67 for wastewater treatment, J. Colloid Interface Sci. 500 (2017) 88–95.
[80] R.Z. Wang, D.L. Huang, Y.G. Liu, C. Zhang, C. Lai, G.M. Zeng, M. Cheng, X.M. Gong, J. Wan, H. Luo, Investigating the adsorption behavior and the relative distribution of Cd^{2+} sorption mechanisms on biochars by different feedstock, Bioresour. Technol. 261 (2018) 265–271.
[81] C. Zhang, G.M. Zeng, D.L. Huang, C. Lai, M. Chen, M. Cheng, W.W. Tang, L. Tang, H.R. Dong, B.B. Huang, X.F. Tan, R.Z. Wang, Biochar for environmental management: mitigating greenhouse gas emissions, contaminant treatment, and potential negative impacts, Chem. Eng. J. 373 (2019) 902–922.
[82] X. Gong, D. Huang, Y. Liu, G. Zeng, R. Wang, J. Wei, C. Huang, P. Xu, J. Wan, C. Zhang, Pyrolysis and reutilization of plant residues after phytoremediation of heavy metals contaminated sediments: For heavy metals stabilization and dye adsorption, Bioresour. Technol. 253 (2018) 64–71.
[83] P. Regmi, J.L.G. Moscoso, S. Kumar, X.Y. Cao, J.D. Mao, G. Schafran, Removal of copper and cadmium from aqueous solution using switchgrass biochar produced via hydrothermal carbonization process, J. Environ. Manage. 109 (2012) 61–69.
[84] B. Sun, F. Lian, Q. Bao, Z. Liu, Z. Song, L. Zhu, Impact of low molecular weight organic acids (LMWOAs) on biochar micropores and sorption properties for sulfamethoxazole, Environ. Pollut. 214 (2016) 142–148.
[85] C. Zhang, C. Lai, G. Zeng, D. Huang, C. Yang, Y. Wang, Y. Zhou, M. Cheng, Efficacy of carbonaceous nanocomposites for sorbing ionizable antibiotic sulfamethazine from aqueous solution, Water Res. 95 (2016) 103–112.
[86] D. Huang, X. Wang, C. Zhang, G. Zeng, Z. Peng, J. Zhou, M. Cheng, R. Wang, Z. Hu, X. Qin, Sorptive removal of ionizable antibiotic sulfamethazine from aqueous solution by graphene oxide-coated biochar nanocomposites: Influencing factors and mechanism, Chemosphere 186 (2017) 414–421.
[87] L. Wu, B.H. Li, M.Z. Liu, Influence of aromatic structure and substitution of carboxyl groups o aromatic acids on their sorption to biochars, Chemosphere 210 (2018) 239–246.
[88] X.F. Tan, S.B. Liu, Y.G. Liu, Y.L. Gu, G.M. Zeng, X.J. Hu, W. Xin, S.H. Liu, L.H. Jiang, Biochar as potential sustainable precursors for activated carbon production: Multiple applications in environmental protection and energy storage, Bioresour. Technol. 227 (2016) 359.
[89] X.F. Tan, Y.G. Liu, Y.L. Gu, Y. Xu, G.M. Zeng, X.J. Hu, S.B. Liu, X. Wang, S.M. Liu, J. Li, Biochar-based nano-composites for the decontamination of wastewater: a review, Bioresour. Technol. 212 (2016) 318–333.
[90] T. Sizmur, T. Fresno, G. Akgul, H. Frost, E. Moreno-Jimenez, Biochar modification to enhance sorption of inorganics from water, Bioresour. Technol. 246 (2017) 34–47.
[91] W. Xiong, J. Tong, Z. Yang, G. Zeng, Y. Zhou, D. Wang, P. Song, R. Xu, C. Zhang, M. Cheng, Adsorption of phosphate from aqueous solution using iron-zirconium modified activated carbon nanofiber: performance and mechanism, J. Colloid Interface Sci. 493 (2017) 17–23.
[92] M.C. Tonucci, L.V.A. Gurgel, S.F. de Aquino, Activated carbons from agricultural byproducts (pine tree and coconut shell), coal, and carbon nanotubes as adsorbents for removal of sulfamethoxazole from spiked aqueous solutions: kinetic and thermodynamic studies, Ind. Crop. Prod. 74 (2015) 111–121.
[93] L. Nielsen, M.J. Biggs, W. Skinner, T.J. Bandosz, The effects of activated carbon surface features on the reactive adsorption of carbamazepine and sulfamethoxazole, Carbon 80 (2014) 419–432.
[94] G. Ersan, O.G. Apul, F. Perreault, T. Karanfil, Adsorption of organic contaminants by graphene nanosheets: a review, Water Res. 126 (2017) 385–398.
[95] S. Zhuang, X. Zhu, J. Wang, Kinetic, equilibrium, and thermodynamic performance of sulfonamides adsorption onto graphene, Environ. Sci. Pollut. 25 (2018) 36615–36623.
[96] T. Kuila, S. Bose, A.K. Mishra, P. Khanra, N.H. Kim, J.H. Lee, Chemical functionalization of graphene and its applications, Prog. Mater Sci. 57 (2012) 1061–1105.
[97] H. Chen, B. Gao, H. Li, Removal of sulfamethoxazole and ciprofloxacin from aqueous solutions by graphene oxide, J. Hazard. Mater. 282 (2015) 201–207.
[98] C. Wang, H. Li, S.H. Liao, H. Zheng, Z.Y. Wang, B. Pan, B.S. Xing, Coadsorption, desorption hysteresis and sorption thermodynamics of sulfamethoxazole and carbamazepine on graphene oxide and graphite, Carbon 65 (2013) 243–251.
[99] W.C. Song, T.T. Yang, X.X. Wang, Y.B. Sun, Y.J. Ai, G.D. Sheng, T. Hayat, X.K. Wang, Experimental and theoretical evidence for competitive interactions of tetracycline and sulfamethazine with reduced graphene oxides, Environ. Sci.: Nano 3 (2016) 1318–1326.
[100] J. Wu, H. Zhao, R. Chen, C. Pham-Huy, X. Hui, H. He, Adsorptive removal of trace sulfonamide antibiotics by water-dispersible magnetic reduced graphene oxide-ferrite hybrids from wastewater, J. Chromatogr B Anal. Technol. Biomed, Life Sci. 1029–1030 (2016) 106–112.
[101] P. Shi, N. Ye, Investigation of the adsorption mechanism and preconcentration of sulfonamides using a porphyrin-functionalized Fe_3O_4-graphene oxide nanocomposite, Talanta 143 (2015) 219–225.
[102] A.M. Kolpak, J.C. Grossman, Azobenzene-functionalized carbon nanotubes as high-energy density solar thermal fuels, Nano Lett. 11 (2011) 3156–3162.
[103] F. Wang, S. Ma, Y. Si, L.F. Dong, X.L. Wang, J. Yao, H.L. Chen, Z.J. Yi, W.C. Yao, B.S. Xing, Interaction mechanisms of antibiotic sulfamethoxazole with various graphene-based materials and multiwall carbon nanotubes and the effect of humic

acid in water, Carbon 114 (2017) 671–678.
[104] J.M. Wei, W.L. Sun, W.Y. Pan, X.Q. Yu, G. Sun, H. Jiang, Comparing the effects of different oxygen-containing functional groups on sulfonamides adsorption by carbon nanotubes: Experiments and theoretical calculation, Chem. Eng. J. 312 (2017) 167–179.
[105] M.I. Nandasiri, S.R. Jambovane, B.P. McGrail, H.T. Schaef, S.K. Nune, Adsorption, separation, and catalytic properties of densified metal-organic frameworks, Coord. Chem. Rev. 311 (2016) 38–52.
[106] W. Xiong, Z. Zeng, X. Li, G. Zeng, R. Xiao, Z. Yang, Y. Zhou, C. Zhang, M. Cheng, L. Hu, C. Zhou, L. Qin, R. Xu, Y. Zhang, Multi-walled carbon nanotube/amino-functionalized MIL-53(Fe) composites: remarkable adsorptive removal of antibiotics from aqueous solutions, Chemosphere 210 (2018) 1061–1069.
[107] W. Xiong, G. Zeng, Z. Yang, Y. Zhou, C. Zhang, M. Cheng, Y. Liu, L. Hu, J. Wan, C. Zhou, R. Xu, X. Li, Adsorption of tetracycline antibiotics from aqueous solutions on nanocomposite multi-walled carbon nanotube functionalized MIL-53(Fe) as new adsorbent, Sci. Total Environ. 627 (2018) 235–244.
[108] K.A. Cychosz, A.J. Matzger, Water stability of microporous coordination polymers and the adsorption of pharmaceuticals from water, Langmuir 26 (2010) 17198–17202.
[109] X. Li, H. Yuan, X. Quan, S. Chen, S. You, Effective adsorption of sulfamethoxazole, bisphenol A and methyl orange on nanoporous carbon derived from metal-organic frameworks, J. Environ. Sci (China) 63 (2018) 250–259.
[110] I. Ahmed, B.N. Bhadra, H.J. Lee, S.H. Jhung, Metal-organic framework-derived carbons: Preparation from ZIF-8 and application in the adsorptive removal of sulfamethoxazole from water, Catal. Today 301 (2018) 90–97.
[111] W. Lertpaitoonpan, S.K. Ong, T.B. Moorman, Effect of organic carbon and pH on soil sorption of sulfamethazine, Chemosphere 76 (2009) 558–564.
[112] P. Srinivasan, A.K. Sarmah, M. Manley-Harris, Co-contaminants and factors affecting the sorption behaviour of two sulfonamides in pasture soils, Environ. Pollut. 180 (2013) 165–172.
[113] S. Thiele-Bruhn, M.O. Aust, Effects of pig slurry on the sorption of sulfonamide antibiotics in soil, Arch. Environ. Contam. Toxicol. 47 (2004) 31–39.
[114] J. Gao, J.A. Pedersen, Adsorption of sulfonamide antimicrobial agents to clay minerals, Environ. Sci. Technol. 39 (2005) 9509–9516.
[115] M.D. Ureñaamate, M. Socíasviciana, E. Gonzálezpradas, M. Saifi, Effects of ionic strength and temperature on adsorption of atrazine by a heat treated kerolite, Chemosphere 59 (2005) 69–74.
[116] I. Braschi, S. Blasioli, L. Gigli, C.E. Gessa, A. Alberti, A. Martucci, Removal of sulfonamide antibiotics from water: Evidence of adsorption into an organophilic zeolite Y by its structural modifications, J. Hazard. Mater. 178 (2010) 218–225.
[117] A.M.L. Fernandez, M. Rendueles, M. Diaz, Competitive Retention of Sulfamethoxazole (SMX) and Sulfamethazine (SMZ) from Synthetic Solutions in a Strong Anionic Ion Exchange Resin, Solvent Extr. Ion Exch. 32 (2014) 763–781.
[118] T. Wang, X. Pan, W. Ben, J. Wang, P. Hou, Z. Qiang, Adsorptive removal of antibiotics from water using magnetic ion exchange resin, J. Environ Sci (China) 52 (2017) 111–117.
[119] A. Martucci, M.A. Cremonini, S. Blasioli, L. Gigli, G. Gatti, L. Marchese, I. Braschi, Adsorption and reaction of sulfachloropyridazine sulfonamide antibiotic on a high silica mordenite: A structural and spectroscopic combined study, Microporous Mesoporous Mater. 170 (2013) 274–286.
[120] S. Blasioli, A. Martucci, G. Paul, L. Gigli, M. Cossi, C.T. Johnston, L. Marchese, I. Braschi, Removal of sulfamethoxazole sulfonamide antibiotic from water by high silica zeolites: A study of the involved host–guest interactions by a combined structural, spectroscopic, and computational approach, J. Colloid and Interface Sci. 419 (2014) 148–159.
[121] Y. Xiang, Z. Xu, Y. Wei, Y. Zhou, X. Yang, Y. Yang, J. Yang, J. Zhang, L. Luo, Z. Zhou, Carbon-based materials as adsorbent for antibiotics removal: Mechanisms and influencing factors, J. Environ. Manage. 237 (2019) 128–138.
[122] C. Ling, X. Li, Z. Zhang, F. Liu, Y. Deng, X. Zhang, A. Li, L. He, B. Xing, High Adsorption of Sulfamethoxazole by an Amine-Modified Polystyrene-Divinylbenzene Resin and Its Mechanistic Insight, Environ. Sci. Technol. 50 (2016) 10015–10023.
[123] Z. Chen, X. Xiao, B. Xing, B. Chen, pH-dependent sorption of sulfonamide antibiotics onto biochars: Sorption mechanisms and modeling, Environ. Pollut. 248 (2019) 48–56.
[124] L. Ji, Y. Wan, S. Zheng, D. Zhu, Adsorption of tetracycline and sulfamethoxazole on crop residue-derived ashes: implication for the relative importance of black carbon to soil sorption, Environ. Sci. Technol. 45 (2011) 5580–5586.
[125] B. Chen, W. Sun, C. Wang, X. Guo, Size-dependent impact of inorganic nanoparticles on sulfamethoxazole adsorption by carbon nanotubes, Chem. Eng. J. 316 (2017) 160–170.
[126] Y. Liu, X.H. Liu, G.D. Zhang, T. Ma, T.Q. Du, Y. Yang, S.Y. Lu, W.L. Wang, Adsorptive removal of sulfamethazine and sulfamethoxazole from aqueous solution by hexadecyl trimethyl ammonium bromide modified activated carbon, Colloids Surf, A 564 (2019) 131–141.
[127] C. Kim, V.R. Panditi, P.R. Gardinali, R.S. Varma, H. Kim, V.K. Sharma, Ferrate promoted oxidative cleavage of sulfonamides: Kinetics and product formation under acidic conditions, Chem. Eng. J. 279 (2015) 307–316.
[128] W.J. Xue, Z.W. Peng, D.L. Huang, G.M. Zeng, X.J. Wen, R. Deng, Y. Yang, X.L. Yan, In situ synthesis of visible-light-driven Z-scheme AgI/Bi_2WO_6 heterojunction photocatalysts with enhanced photocatalytic activity, Ceram. Int. 45 (2019) 6340–6349.
[129] O. Cindy, D.L.D. Lima, S.C. Patrícia, C. Vania, O. Marta, V.I. Esteves, Photodegradation of sulfamethoxazole in environmental samples: The role of pH, organic matter and salinity, Sci. Total Environ. 648 (2019) 1403–1410.
[130] A.L. Boreen, W.A. Arnold, K. McNeill, Photochemical fate of sulfa drugs in the aquatic environment: sulfa drugs containing five-membered heterocyclic groups, Environ. Sci. Technol. 38 (2004) 3933–3940.
[131] L. Zhou, X. Yang, Y. Ji, J. Wei, Sulfate radical-based oxidation of the antibiotics sulfamethoxazole, sulfisoxazole, sulfathiazole, and sulfamethizole: The role of five-membered heterocyclic rings, Sci. Total Environ. 692 (2019) 201–208.
[132] A. Acosta-Rangel, M. Sanchez-Polo, A.M.S. Polo, J. Rivera-Utrilla, M.S. Berber-Mendoza, Sulfonamides degradation assisted by UV, UV/H_2O_2 and $UV/K_2S_2O_8$: Efficiency, mechanism and byproducts cytotoxicity, J. Environ. Manage. 225 (2018) 224–231.
[133] P. Ge, H. Yu, J. Chen, J. Qu, Y. Luo, Photolysis mechanism of sulfonamide moiety in five-membered sulfonamides: a DFT study, Chemosphere 197 (2018) 569–575.
[134] P. Neta, R.E. Huie, A.B. Ross, Rate constants for reactions of inorganic radicals in aqueous solution, J. Phys. Chem. Ref. Data 17 (1988) 1027–1284.
[135] G.V. Buxton, C.L. Greenstock, W.P. Helman, A.B. Ross, Critical Review of rate constants for reactions of hydrated electrons, hydrogen atoms and hydroxyl radicals (·OH/·O− in Aqueous Solution, J. Phys. Chem. Ref. Data 17 (1988) 513–886.
[136] Y. Xiao, L. Zhang, W. Zhang, K.Y. Lim, R.D. Webster, T.T. Lim, Comparative evaluation of iodoacids removal by UV/persulfate and UV/H_2O_2 processes, Water Res. 102 (2016) 629–639.
[137] M.G. Antoniou, H.R. Andersen, Comparison of $UVC/S2O_8^{2-}$ with UVC/H_2O_2 in terms of efficiency and cost for the removal of micropollutants from groundwater, Chemosphere 119 (2015) S81–S88.
[138] Y. Yang, X. Lu, J. Jiang, J. Ma, G. Liu, Y. Cao, W. Liu, J. Li, S. Pang, X. Kong, C. Luo, Degradation of sulfamethoxazole by UV, UV/H_2O_2 and UV/persulfate (PDS): Formation of oxidation products and effect of bicarbonate, Water Res. 118 (2017) 196–207.
[139] C. Cui, L. Jin, L. Jiang, Q. Han, K. Lin, S. Lu, D. Zhang, G. Cao, Removal of trace level amounts of twelve sulfonamides from drinking water by UV-activated peroxymonosulfate, Sci. Total Environ. 572 (2016) 244–251.
[140] Y. Ji, Y. Yang, L. Zhou, L. Wang, J. Lu, C. Ferronato, J.M. Chovelon, Photodegradation of sulfasalazine and its human metabolites in water by UV and UV/peroxydisulfate processes, Water Res. 133 (2018) 299–309.
[141] R. Zhang, P. Sun, T.H. Boyer, L. Zhao, C.H. Huang, Degradation of pharmaceuticals and metabolite in synthetic human urine by UV, UV/H_2O_2, and UV/PDS, Environ. Sci. Technol. 49 (2015) 3056–3066.
[142] C. Zhou, C. Lai, P. Xu, G. Zeng, D. Huang, C. Zhang, M. Cheng, L. Hu, J. Wan, Y. Liu, W. Xiong, Y. Deng, M. Wen, In Situ Grown $AgI/Bi_{12}O_{17}Cl_2$ Heterojunction Photocatalysts for Visible Light Degradation of Sulfamethazine: Efficiency, Pathway, and Mechanism, ACS Sustainable Chem. Eng. 6 (2018) 4174–4184.
[143] Y. Yang, Z. Zeng, G. Zeng, D. Huang, R. Xiao, C. Zhang, C. Zhou, W. Xiong, W. Wang, M. Cheng, W. Xue, H. Guo, X. Tang, D. He, Ti_3C_2 Mxene/porous g-C_3N_4 interfacial Schottky junction for boosting spatial charge separation in photocatalytic H_2O_2 production, Appl. Catal., B 258 (2019).
[144] X.J. Yuan, D. Floresyona, P.H. Aubert, T.T. Bui, S. Remita, S. Ghosh, F. Brisset, F. Goubard, H. Remita, Photocatalytic degradation of organic pollutant with polypyrrole nanostructures under UV and visible light, Appl. Catal., B 242 (2019) 284–292.
[145] N.D.L. Cruz, R.F. Dantas, J. Giménez, S. Esplugas, Photolysis and TiO_2 photocatalysis of the pharmaceutical propranolol: Solar and artificial light, Appl. Catal., B 130 (2013) 249–256.
[146] C.Y. Zhou, C. Lai, C. Zhang, G.M. Zeng, D.L. Huang, M. Cheng, L. Hu, W.P. Xiong, M. Chen, J.J. Wang, Y. Yang, L.B. Jiang, Semiconductor/boron nitride composites: Synthesis, properties, and photocatalysis applications, Appl. Catal., B 238 (2018) 6–18.
[147] J.R. Kim, E. Kan, Heterogeneous photocatalytic degradation of sulfamethoxazole in water using a biochar-supported TiO_2 photocatalyst, J. Environ. Manage. 180 (2016) 94–101.
[148] E. Grilla, A. Petala, Z. Frontistis, I.K. Konstantinou, D.I. Kondarides, D. Mantzavinos, Solar photocatalytic abatement of sulfamethoxazole over Ag_3PO_4/WO_3 composites, Appl. Catal., B 231 (2018) 73–81.
[149] J. Theerthagiri, S. Chandrasekaran, S. Salla, V. Elakkiya, R.A. Senthil, P. Nithyadharseni, T. Maiyalagan, K. Micheal, A. Ayeshamariam, M.V. Arasu, N.A. Al-Dhabi, H.-S. Kim, Recent developments of metal oxide based heterostructures for photocatalytic applications towards environmental remediation, J. Solid State Chem. 267 (2018) 35–52.
[150] Y. Yang, C. Zhang, D. Huang, G. Zeng, J. Huang, C. Lai, C. Zhou, W. Wang, H. Guo, W. Xue, R. Deng, M. Cheng, W. Xiong, Boron nitride quantum dots decorated ultrathin porous g-C_3N_4: Intensified exciton dissociation and charge transfer for promoting visible-light-driven molecular oxygen activation, Appl. Catal., B 245 (2019) 87–99.
[151] Y. Yang, C. Zhang, C. Lai, G. Zeng, D. Huang, M. Cheng, J. Wang, F. Chen, C. Zhou, W. Xiong, BiOX (X = Cl, Br, I) photocatalytic nanomaterials: Applications for fuels and environmental management, Adv Colloid Interface Sci. 254 (2018) 76–93.
[152] C. Martínez, C.L. M., M.I. Fernández, J.A. Santaballa, J. Faria, Kinetics and mechanism of aqueous degradation of carbamazepine by heterogeneous photocatalysis using nanocrystalline TiO2 , ZnO and multi-walled carbon nanotubes–anatase composites, Appl. Catal., B 102 (2011) 563-571.
[153] Y.F. Chen, C.J. Zhang, W.X. Huang, Y. Situ, H. Huang, Multimorphologies nano-ZnO preparing through a simple solvothermal method for photocatalytic application, Mater Lett. 141 (2015) 294–297.
[154] M. Cheng, G. Zeng, D. Huang, L. Cui, P. Xu, C. Zhang, Y. Liu, Hydroxyl radicals based advanced oxidation processes (AOPs) for remediation of soils contaminated with organic compounds: a review, Chem. Eng. J. 284 (2016) 582–598.
[155] E. Ioannidou, Z. Frontistis, M. Antonopoulou, D. Venieri, I. Konstantinou, D.I. Kondarides, D. Mantzavinos, Solar photocatalytic degradation of

sulfamethoxazole over tungsten-Modified TiO_2, Chem. Eng. J. 318 (2017) 143–152.
[156] W. Zhu, F. Sun, R. Goei, Y. Zhou, Construction of WO_3-g-C_3N_4 composites as efficient photocatalysts for pharmaceutical degradation under visible light, Catal. Sci. Technol. 7 (2017) 2591–2600.
[157] W. Zhu, Z. Li, C. He, S. Faqian, Y. Zhou, Enhanced photodegradation of sulfamethoxazole by a novel WO_3-CNT composite under visible light irradiation, J. Alloys Compds. 754 (2018) 153–162.
[158] H. Yi, D.L. Huang, L. Qin, G.M. Zeng, C. Lai, M. Cheng, S.J. Ye, B. Song, X.Y. Ren, X.Y. Guo, Selective prepared carbon nanomaterials for advanced photocatalytic application in environmental pollutant treatment and hydrogen production, Appl. Catal., B 239 (2018) 408–424.
[159] R.Z. Wang, D.L. Huang, Y.G. Liu, C. Zhang, C. Lai, X. Wang, G.M. Zeng, X.M. Gong, A. Duan, Q. Zhang, P. Xu, Recent advances in biochar-based catalysts: Properties, applications and mechanisms for pollution remediation, Chem. Eng. J. 371 (2019) 380–403.
[160] D. He, C. Zhang, G. Zeng, Y. Yang, D. Huang, L. Wang, H. Wang, A multifunctional platform by controlling of carbon nitride in the core-shell structure: From design to construction, and catalysis applications, Appl. Catal., B 258 (2019).
[161] W.J. Wang, P. Xu, M. Chen, G.M. Zeng, C. Zhang, C.Y. Zhou, Y. Yang, D.L. Huang, C. Lai, M. Cheng, L. Hu, W.P. Xiong, H. Guo, M. Zhou, Alkali Metal-Assisted Synthesis of Graphite Carbon Nitride with Tunable Band-Gap for Enhanced Visible-Light-Driven Photocatalytic Performance, ACS Sustainable Chem. Eng. 6 (2018) 15503–15516.
[162] L. Qin, D.L. Huang, P. Xu, G.M. Zeng, C. Lai, Y.K. Fu, H. Yi, B.S. Li, C. Zhang, M. Cheng, C.Y. Zhou, X.F. Wen, In-situ deposition of gold nanoparticles onto polydopamine-decorated g-C_3N_4 for highly efficient reduction of nitroaromatics in environmental water purification, J. Colloid and Interface Sci. 534 (2019) 357–369.
[163] W. Wang, Z. Zeng, G. Zeng, C. Zhang, R. Xiao, C. Zhou, W. Xiong, Y. Yang, L. Lei, Y. Liu, D. Huang, M. Cheng, Y. Yang, Y. Fu, H. Luo, Y. Zhou, Sulfur doped carbon quantum dots loaded hollow tubular g-C_3N_4 as novel photocatalyst for destruction of Escherichia coli and tetracycline degradation under visible light, Chem. Eng. J. 378 (2019).
[164] N. Chen, Y. Huang, X. Hou, Z. Ai, L. Zhang, Photochemistry of hydrochar: reactive oxygen species generation and sulfadimidine degradation, Environ. Sci. Technol. 51 (2017) 11278–11287.
[165] D.L. Huang, Y. Wang, C. Zhang, G.M. Zeng, C. Lai, J. Wan, L. Qin, Y. Zeng, Influence of morphological and chemical features of biochar on hydrogen peroxide activation: implications on sulfamethazine degradation, RSC Adv. 6 (2016) 73186–73196.
[166] Y.L. Song, J.Y. Tian, S.S. Gao, P.H. Shao, J.Y. Qi, F.Y. Cui, Photodegradation of sulfonamides by g-C_3N_4 under visible light irradiation: Effectiveness, mechanism and pathways, Appl. Catal., B 210 (2017) 88–96.
[167] C.Y. Zhou, D.L. Huang, P. Xu, G.M. Zeng, J.H. Huang, T.Z. Shi, C. Lai, C. Zhang, M. Cheng, Y. Lu, A. Duan, W.P. Xiong, M. Zhou, Efficient visible light driven degradation of sulfamethazine and tetracycline by salicylic acid modified polymeric carbon nitride via charge transfer, Chem. Eng. J. 370 (2019) 1077–1086.
[168] W.Y. Zhu, F.Q. Sun, R. Goei, Y. Zhou, Facile fabrication of RGO-WO_3 composites for effective visible light photocatalytic degradation of sulfamethoxazole, Appl. Catal., B 207 (2017) 93–102.
[169] N. Wang, X. Li, Y. Yang, T. Guo, X. Zhuang, S. Ji, T. Zhang, Y. Shang, Z. Zhou, Enhanced photocatalytic degradation of sulfamethazine by Bi-doped TiO_2 nanocomposites supported by powdered activated carbon under visible light irradiation, Sep. Purif. Technol. 211 (2019) 673–683.
[170] G. Di, Z. Zhu, H. Zhang, J. Zhu, Y. Qiu, D. Yin, S. Kuppers, Visible-light degradation of sulfonamides by Z-scheme ZnO/g-C_3N_4 heterojunctions with amorphous Fe2O3 as electron mediator, J. Colloid Interface Sci. 538 (2018) 256–266.
[171] C.Y. Zhou, P. Xu, C. Lai, C. Zhang, G.M. Zeng, D.L. Huang, M. Cheng, L. Hu, W.P. Xiong, X.F. Wen, L. Qin, J.L. Yuan, W.J. Wang, Rational design of graphic carbon nitride copolymers by molecular doping for visible-light-driven degradation of aqueous sulfamethazine and hydrogen evolution, Chem. Eng. J. 359 (2019) 186–196.
[172] C. Min, G. Zeng, D. Huang, L. Cui, L. Yang, P. Xu, Z. Chen, W. Jia, H. Liang, W. Xiong, Salicylic acid–methanol modified steel converter slag as heterogeneous Fenton-like catalyst for enhanced degradation of alachlor, Chem. Eng. J. 327 (2017) 686–693.
[173] Y. Liu, M. Cheng, Z. Liu, G. Zeng, H. Zhong, M. Chen, C. Zhou, W. Xiong, B. Shao, B. Song, Heterogeneous Fenton-like catalyst for treatment of rhamnolipid-solubilized hexadecane wastewater, Chemosphere 236 (2019) 124387.
[174] E. Cuervo Lumbaque, R. Wielens Becker, D. Salmoria Araujo, A. Dallegrave, T. Ost Fracari, V. Lavayen, C. Sirtori, Degradation of pharmaceuticals in different water matrices by a solar homo/heterogeneous photo-Fenton process over modified alginate spheres, Environ. Sci. Pollut. 26 (2019) 6532–6544.
[175] R. Zhuan, J. Wang, Enhanced degradation and mineralization of sulfamethoxazole by integrating gamma radiation with Fenton-like processes, Radiat. Phys. Chem. 166 (2020).
[176] M. Velásquez, I.P. Santander, D.R. Contreras, J. Yáñez, C. Zaror, R.A. Salazar, M. Pérez-Moya, H.D. Mansilla, Oxidative degradation of sulfathiazole by Fenton and photo-Fenton reactions, J. Environ. Sci. Health., Part A 49 (2014) 661–670.
[177] J.I. Martinez-Costa, J. Rivera-Utrilla, R. Leyva-Ramos, M. Sanchez-Polo, I. Velo-Gala, A.J. Mota, Individual and simultaneous degradation of the antibiotics sulfamethoxazole and trimethoprim in aqueous solutions by Fenton, Fenton-like and photo-Fenton processes using solar and UV radiations, J. Photoch. Photobio. A 360 (2018) 95–108.
[178] T. Zhou, X.H. Wu, Y.R. Zhang, J.F. Li, T.T. Lim, Synergistic catalytic degradation of antibiotic sulfamethazine in a heterogeneous sonophotolytic goethite/oxalate Fenton-like system, Appl. Catal., B 136 (2013) 294–301.
[179] I. Michael, E. Hapeshi, C. Michael, A.R. Varela, S. Kyriakou, C.M. Manaia, D. Fatta-Kassinos, Solar photo-Fenton process on the abatement of antibiotics at a pilot scale: Degradation kinetics, ecotoxicity and phytotoxicity assessment and removal of antibiotic resistant enterococci, Water Res. 46 (2012) 5621–5634.
[180] A. Mirzaei, Z. Chen, F. Haghighat, L. Yerushalmi, Removal of pharmaceuticals from water by homo/heterogonous Fenton-type processes - A review, Chemosphere 174 (2017) 665–688.
[181] D. Klauson, N. Romero Sarcos, M. Krichevskaya, E. Kattel, N. Dulova, T. Dedova, M. Trapido, Advanced oxidation processes for sulfonamide antibiotic sulfamethizole degradation: Process applicability study at ppm level and scale-down to ppb level, J. Environ. Chem. Eng. 7 (2019).
[182] K. Roy, V.S. Moholkar, Sulfadiazine degradation using hybrid AOP of heterogeneous Fenton/persulfate system coupled with hydrodynamic cavitation, Chem. Eng. J. (2019).
[183] N. Barhoumi, N. Oturan, H. Olvera-Vargas, E. Brillas, A. Gadri, S. Ammar, M.A. Oturan, Pyrite as a sustainable catalyst in electro-Fenton process for improving oxidation of sulfamethazine. Kinetics, mechanism and toxicity assessment, Water Res. 94 (2016) 52–61.
[184] M. Cheng, Y. Liu, D. Huang, C. Lai, G. Zeng, J. Huang, Z. Liu, C. Zhang, C. Zhou, L. Qin, W. Xiong, H. Yi, Y. Yang, Prussian blue analogue derived magnetic Cu-Fe oxide as a recyclable photo-Fenton catalyst for the efficient removal of sulfamethazine at near neutral pH values, Chem. Eng. J. 362 (2019) 865–876.
[185] J. Gao, S. Wu, Y. Han, F. Tan, Y. Shi, M. Liu, X. Li, 3D mesoporous $CuFe_2O_4$ as a catalyst for photo-Fenton removal of sulfonamide antibiotics at near neutral pH, J. Colloid Interface Sci. 524 (2018) 409–416.
[186] S. Ignasi, B. Enric, M.A. Oturan, M.A. Rodrigo, P. Marco, Electrochemical advanced oxidation processes: today and tomorrow. A review, Environ. Sci. Pollut. Res. 21 (2014) 8336–8367.
[187] Y. Zhu, S. Qiu, F. Deng, Y. Zheng, K. Li, F. Ma, D. Liang, Enhanced degradation of sulfathiazole by electro-Fenton process using a novel carbon nitride modified electrode, Carbon 145 (2019) 321–332.
[188] F. Deng, S. Li, M. Zhou, Y. Zhu, S. Qiu, K. Li, F. Ma, J. Jiang, A biochar modified nickel-foam cathode with iron-foam catalyst in electro-Fenton for sulfamerazine degradation, Appl. Catal., B 256 (2019).
[189] D.H. Guo, R. Shibuya, C. Akiba, S. Saji, T. Kondo, J. Nakamura, Active sites of nitrogen-doped carbon materials for oxygen reduction reaction clarified using model catalysts, Science 351 (2016) 361–365.
[190] C.H. Wu, J.T. Wu, Y.H. Lin, Mineralization of sulfamethizole in photo-Fenton and photo-Fenton-like systems, Water Sci. Technol. 73 (2016) 746–750.
[191] M. Cheng, G. Zeng, D. Huang, C. Lai, Y. Liu, C. Zhang, J. Wan, L. Hu, C. Zhou, W. Xiong, Efficient degradation of sulfamethazine in simulated and real wastewater at slightly basic pH values using Co-SAM-SCS/H_2O_2 Fenton-like system, Water Res. 138 (2018) 7–18.
[192] Z. Wan, J. Wang, Degradation of sulfamethazine using Fe_3O_4-Mn_3O_4/reduced graphene oxide hybrid as Fenton-like catalyst, J. Hazard. Mater. 324 (2017) 653–664.
[193] M. Jiang, Q. Zhang, Y. Ji, D. Kong, J. Lu, X. Yin, Q. Zhou, C. Ferronato, J.M. Chovelon, Transformation of antimicrobial agent sulfamethazine by peroxymonosulfate: Radical vs. nonradical mechanisms, Sci. Total Environ. 636 (2018) 864–871.
[194] A. Ledjeri, I. Yahiaoui, H. Kadji, F. Aissani-Benissad, A. Amrane, F. Fourcade, Combination of the Electro/Fe^{3+}/peroxydisulfate (PDS) process with activated sludge culture for the degradation of sulfamethazine, Environ. Toxicol. Pharmacol. 53 (2017) 34–39.